ANL-75-46

ANL-75-46

CHEMICAL ENGINEERING DIVISION

PHYSICAL INORGANIC CHEMISTRY ANNUAL REPORT

July 1974—June 1975

by

M. Blander, C. J. Cajigas, H. S. Huang,
G. H. Kucera, A. E. Martin, G. Papatheodorou,
T. A. Renner, M. L. Saboungi, J. R. Selman,
R. K. Steunenberg, F. A. Cafasso, and L. Burris

RMC-AUA-USERDA

ARGONNE NATIONAL LABORATORY, ARGONNE, ILLINOIS

Prepared for the U. S. ENERGY RESEARCH
AND DEVELOPMENT ADMINISTRATION
under Contract W-31-109-Eng-38

Printed in the United States of America
Available from
National Technical Information Service
U. S. Department of Commerce
5285 Port Royal Road
Springfield, Virginia 22161
Price: Printed Copy \$5.50; Microfiche \$2.25

Distribution Category:
Chemistry (UC-4)

ANL-75-46

ARGONNE NATIONAL LABORATORY
9700 South Cass Avenue
Argonne, Illinois 60439

CHEMICAL ENGINEERING DIVISION

PHYSICAL INORGANIC CHEMISTRY ANNUAL REPORT

July 1974—June 1975

by

M. Blander, C. J. Cajigas, H. S. Huang,
G. H. Kucera, A. E. Martin, G. Papatheodorou,
T. A. Renner, M. L. Saboungi, J. R. Selman,
R. K. Steunenberg, F. A. Cafasso, and L. Burris

Previous reports in this series

ANL-7878	July—December 1971
ANL-7923	January—June 1972
ANL-7978	July—December 1972
ANL-8023	January—June 1973
ANL-8123	July 1973—June 1974

TABLE OF CONTENTS

Page

LIST OF FIGURES

LIST OF TABLES

CHEMICAL ENGINEERING DIVISION
PHYSICAL INORGANIC CHEMISTRY ANNUAL REPORT

July 1974—June 1975

by

M. Blander, C. J. Cajigas, H. S. Huang,
G. H. Kucera, A. E. Martin, G. Papatheodorou,
T. A. Renner, M. L. Saboungi, J. R. Selman,
R. K. Steunenberg, F. A. Cafasso, and L. Burris

ABSTRACT

Thermal conductivity measurements of methanol vapor were made in a hot-wire cell at temperatures ranging from 306-345 K and pressures from 80-760 torr. The data on thermal conductivity (λ) could be fitted to equations of the form $\lambda = \lambda_o + Ap^3$, where p is pressure. The 0.2 to 0.5% of tetrametric alcohol species indicated by the results enhance thermal conductivities about 30%. Emf measurements of the activities of Li in Li-Mg alloys indicate small negative deviations from ideal behavior. These activities, as well as the activities of Mg calculated using the Gibbs-Duhem equation, differ significantly from the less reliable data of Mashovets and Puchkov. Conformal ionic solution theory has been extended to fourth order for additive ternary molten salt systems (AX-BX-CX). All of the terms but one can be calculated from the three subsidiary binaries and the one unknown term is probably negligible. Enthalpy of mixing measurements of alkali nitrates appear to be consistent with the theory. Solution behavior in these ternary systems is not as simple as is usually assumed in the literature. A miscibility isotherm at 540°C for the Na,Ag$||NO_3$,Br system measured by a visual titration method appears to be consistent with theoretical considerations. The laser-raman spectrometer has been improved for planned studies of salt vapors. Certain phase relationships in the systems, Li-Fe-S, Li-Cu-Fe-S, and Li-Co-Fe-S at 400°C, which are of interest to the lithium/metal sulfide battery program, were investigated. Methods were developed for the synthesis of a Li-K-Fe-S phase that is formed in the positive electrodes of Li/FeS cells. Emf measurements of Li-Al alloys relative to lithium were made to obtain further data on the Li-Al phase diagram and on the thermodynamics of the Li-Al system. A value for the free energy of formation of Li_2C_2 was obtained from emf measurements. A study of the crystallization of metastable supercooled molten $MgO-SiO_2$ droplets was made as a function of composition and temperatures. The degree of supercooling, which ranged from 400-750°C, could be correlated with crystal textures and other features of the resultant spherules. The results place significant limitations on current theories of the origin of meteorites and of the early history of the solar system. An examination of the diffusion of oxygen isotopes in mineral grains indicates that the oxygen isotope anomalies found by Clayton *et al.*, in inclusions in the Allende meteorite appear to have been formed by diffusion of ^{17}O and ^{18}O into materials very low in these isotopes. The result is consistent with our earlier conclusions that these inclusions had been liquid.

SUMMARY

Physical Properties of Associating Gases

Thermal Conductivity of Associating Gases. Thermal conductivities of methanol were measured at temperatures ranging from 306-345 K using a thick hot wire cell. The measured thermal conductivities could be fit to equations of the form $\lambda = \lambda_o + Ap^3$ where the values of λ_o and A are given by

$$\lambda_o \times 10^5 = -13.95_7 + 1.029_4 T^{1/2}$$

and

$$\ln(A \times 10^5) = -55.1864 + \frac{12226}{T}$$

The results indicate the presence of a tetrameric alcoholic species, and association constants deduced from the data are given by

$$RT \ln K_{14}(\text{atm}^{-3}) = 24{,}200 - 81.3T$$

At saturation there is about 0.2% tetramer at 307 K and 0.5% at 345 K.

Electromotive Force Measurements in Molten Alkali Metal Alloys

Electromotive Force Measurements in Molten Li-Mg Alloys. Emf measurements of the activity of lithium in molten Li-Mg alloys were made at 670, 735, 830, and 887 K using the cell

$$\text{Li(liq. in Feltmetal)} \left| \begin{array}{c} \text{LiF-LiCl} \\ \text{(eutectic)} \\ \text{or} \\ \text{LiCl-KCl} \\ \text{(eutectic)} \end{array} \right| \text{Li-Mg(liq.)}$$

Activities of magnesium at 887 K were calculated from the measured activities of lithium. The small negative deviations from ideal solution behavior of both components differ significantly from the less reliable results of Mashovets and Puchkov. Activities of solid Li-Mg alloys at the solidus deduced from our data also exhibit small negative deviations from ideality.

Chemistry of Molten Salts and Their Vapors

Conformal Ionic Solution Theory for Additive Ternary Systems. Conformal ionic solution theory has been extended to fourth order terms for additive

ternary molten salt systems (AX-BX-CX or AX-AY-AZ). The resulting equation for the excess Helmholtz free energy of mixing, for example, is

$$\Delta A_m^{XS} = \sum_{i<j}\sum a_{ij}X_iX_j + \sum_{i\neq j}\sum b_{ij}X_i^2X_j + \sum_{i<j}\sum c_{ij}X_i^2X_j^2$$

$$+ AX_1X_2X_3 + \sum_{\substack{i=1 \\ i\neq j<k}}^{3} B_iX_i^2X_jX_k$$

The coefficients a_{ij}, b_{ij} and c_{ij} can be determined from measurements on the three subsidiary binaries, $B_i = 2(c_{ij}c_{ik})^{1/2}$, and A can be approximated by

$$A \cong (b_{12}^{1/3} + b_{13}^{1/3})(b_{21}^{1/3} + b_{23}^{1/3})(b_{13}^{1/3} + b_{23}^{1/3})$$

The results are in agreement with enthalpy of mixing data on alkali nitrates. The equations indicate that solution behavior in these systems is more complex than is usually assumed in the literature.

Miscibility Gaps in Reciprocal Salt Systems. A miscibility isotherm at 813 K was measured in the Na,Ag||NO_3,Br system using a visual titration technique. The miscibility gap is extensive and is not much smaller than that determined previously at 793 K. The size and temperature variations appear to be consistent with expectations from conformal ionic solution theory for reciprocal systems.

Salt Vapor Studies. The optics of the laser-raman spectrometer have been improved and a new furnace constructed for the study of salt vapors. We plan a study of associated salt vapor species containing "acidic gases" such as $AlCl_3$ and $FeCl_3$.

Physical Chemistry of Alkali Metal-Sulfide Battery Systems

Phase Studies of Iron Sulfide Electrodes. Three ternary solid phases in the system Li-Fe-S have been identified in the FeS_2 electrodes of lithium/iron sulfide cells. There appears to be a liquid region in the Li-Fe-S system that extends from the Li-S side to the Fe-S side of the ternary phase diagram; however, this liquid region lies outside the range of compositions and temperatures involved in the operation of cells. In the Li-Cu-Fe-S system at 400°C, two or possibly three compounds of Li_2S with Cu_2S were found, and Cu_2S proved to be significantly soluble in Li_2S and in Li_2FeS_2. No reactions were observed between Li_2S and cobalt sulfides at 400°C. A procedure was developed for the chemical synthesis of a phase that is found in partially charged or discharged FeS electrodes. This phase is basically a Li-K-Fe-S compound, which is formed by a reaction involving the molten LiCl-KCl electrolyte.

Emf Studies of Lithium-Aluminum Alloys. The emf of lithium-aluminum alloys, relative to lithium metal, decreases from 296 to 24 mV at 427°C (700 K), over the composition range of the β phase (48-56 at. % lithium). A solid Li_3Al_2-liquid, two-phase region of high lithium activity was found at lithium concentrations above 60 at. % in the temperature range from 390 to 522°C. The compounds, Li_2Al and Li_9Al_4, which are reported to exist at room temperature, were not observed at these temperatures. The lithium-rich liquidus composition at 470°C is about 2 at. % richer in lithium than the value indicated in standard compilations.

Electrochemistry of Lithium Carbide. Potentials that were measured at a graphite electrode in molten LiCl-KCl eutectic saturated with Li_2C_2 did not agree with literature values for the free energy of formation of Li_2C_2, which, themselves, are in conflict. A ΔG_f° value of about -26 kcal/mol at 700 K was obtained from emf data. Cyclic voltammetry studies of molten-salt electrolytes containing additions of Li_2C_2 indicate that $C_2^=$ ions are discharged at an unexpectedly high value of 2.8 V *vs.* Li+/Li°.

Meteoritic Studies

Supercooling of Laser-Melted Silicates: Application to the Formation of Meteorites. Laser-melted $MgO-SiO_2$ spherules were supercooled in a furnace to 400-750°C below their liquidus temperatures before crystallizing. The resulting textures, morphologies, and crystal sizes observed in thin sections were correlated with the degree of supercooling. The spherules bear striking resemblances to meteoritic chondrules, and our results place important constraints on the origins of chondrules and meteorites in the early solar system.

Oxygen Isotopes in Refractory Inclusions in Allende. Recent measurements of oxygen isotope anomalies in refractory inclusions in the meteorite Allende by Clayton *et al.* indicate that deviations from an ^{17}O isotope standard, δ_{17}, appear to vary linearly with deviations from an ^{18}O isotope standard, δ_{18}, with a slope slightly less than unity. This surprising result has been interpreted to mean that these inclusions had never been liquid. An analysis of the diffusion of ^{18}O and ^{17}O at moderately high temperatures into solid minerals highly depleted in these isotopes indicates that the anomalies measured by Clayton *et al.* were formed by different extents of diffusion of these isotopes into different mineral grains having different values of D/a^2. Our analysis is in close agreement with the measurements whereas the mechanism postulated by Clayton *et al.* is not. We conclude that the measurements are consistent with our earlier conclusions that these refractory inclusions had been liquid.

I. PHYSICAL PROPERTIES OF ASSOCIATING GASES
(M. Blander)

The enhanced thermal conductivities and heat capacities of associating gases, as well as their nonideal PVT behavior, may prove useful for improved working fluids in power cycles. Measurements of the thermophysical properties of such gases are under way to gain an understanding of their fundamental bonding behavior, to determine which aggregated species are formed, and to obtain data needed for analysis of their potential applications as working fluids.

A. Thermal Conductivity of Associating Gases
(T. A. Renner and G. H. Kucera)

We have measured the thermal conductivity of methancl vapor between 306 K and 345 K in the pressure range 80-760 torr. The experimental technique employed was a modification of the hot-wire cell method of Coffin and O'Neal.[1] Our hot-wire cell consisted of a soft glass tube 10 cm in length with an I.D. of 0.5 cm. A uniform platinum wire of 0.51 mm dia was mounted under tension along the axis of the glass cylinder by positioning it through the center of two platinum caps which were sealed at each end of the glass tube. A regulated constant current of 2.25 A was passed through the wire in order to produce a radial and an axial thermal gradient in the methanol vapor. The pressure in the cell was monitored with a thin-film strain-gage pressure transducer calibrated against a mercury manometer.

The thermal conductivity cell was calibrated against reference gases of known conductivity, namely, helium, nitrogen, and argon. The voltage drop across the cell assembly was found to vary linearly with the reciprocal of the thermal conductivity of the reference gases. Experimental values for methanol lay between those for nitrogen and argon. The precision of the data accumulated with this apparatus was estimated to be approximately $\pm 0.5\%$.

The experimental thermal conductivities of methanol are shown in Figs. 1-5 for the five temperatures studied. At each temperature, the data were fitted to polynomial functions of the pressure with two, three, and four

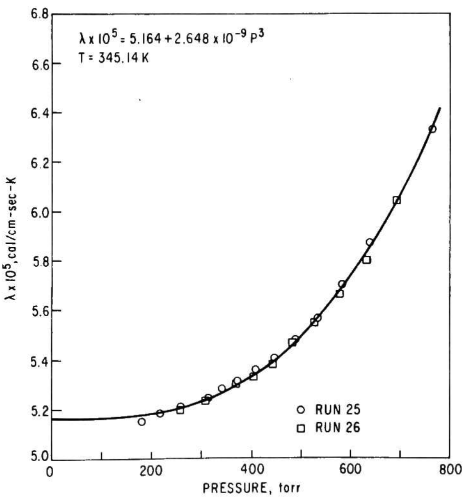

Fig. 1.

Thermal Conductivity of Methanol Vapor as a Function of Pressure at 345.14 K

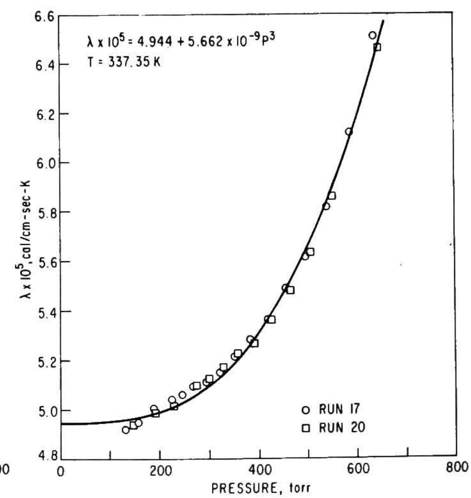

Fig. 2.

Thermal Conductivity of Methanol Vapor as a Function of Pressure at 337.35 K

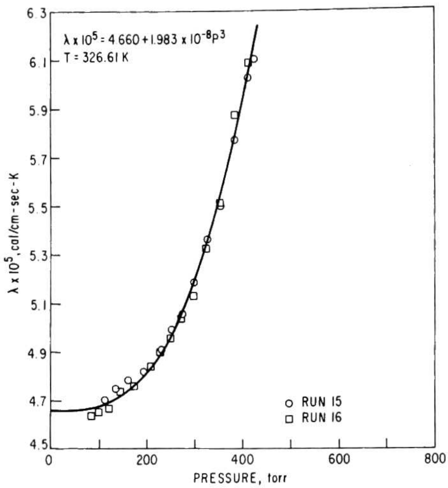

Fig. 3.

Thermal Conductivity of Methanol Vapor as a Function of Pressure at 326.61 K

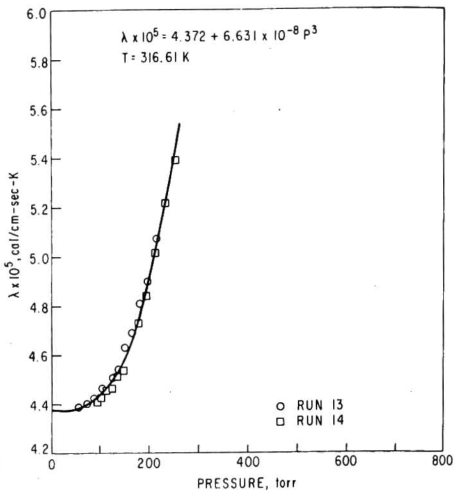

Fig. 4.

Thermal Conductivity of Methanol Vapor as a Function of Pressure at 316.61 K

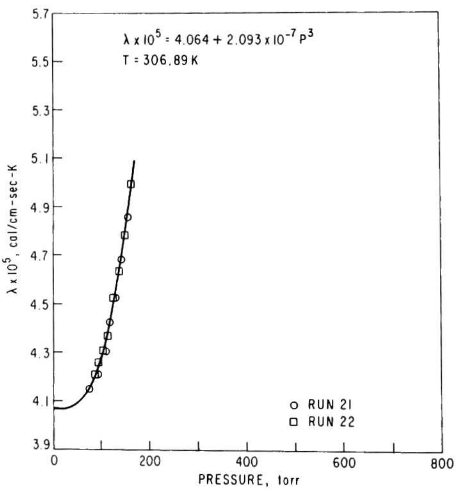

Fig. 5.

Thermal Conductivity of Methanol Vapor as a Function of Pressure at 306.89 K parameters. The data were best fitted to the following equation

$$\lambda = \lambda_o + Ap^3 \tag{1}$$

where λ is the thermal conductivity of methanol expressed in cal cm^{-1} sec^{-1} K^{-1}, λ_o is the "frozen" conductivity (*i.e.*, the thermal conductivity in the absence of the association reaction), and Ap^3 is the enhancement of the thermal conductivity due to the formation of methanol tetramers (the degree of polymerization,[2] n, appears in the pressure-dependent term of Eq. 1 as p^{n-1}). Inclusion of a dimer term, a term linear in p, in Eq. 1 does not lead to an improvement in the fit; in fact, for two of the temperatures studied, the uncertainty in the coefficient of the dimer term was much greater in magnitude than the coefficient itself. It is evident from our results that, in the case of methanol, the thermal conductivity is most sensitive to the existence of the tetramer. Equation 1 reproduces experimental thermal conductivities with an average error of about $\pm 0.5\%$.

The dependence of λ_o on temperature is given by

$$\lambda_o \times 10^5 = -13.95_7 + 1.029_4\ T^{1/2} \tag{2}$$

whereas the temperature dependence of the coefficient, A, in Eq. 1 may be written

$$\ln\ (A \times 10^5) = -55.1864 + \frac{12226}{T} \tag{3}$$

between 306 K and 345 K. Equations 2 and 3 were determined by the method of least squares from values of λ_o and A was derived from experimental results at each temperature. The A-coefficient may also be calculated from the theoretical expression[2]

$$A = \left(\frac{pD_{14}}{RT}\right)\left(\frac{\Delta H_{14}^2}{RT^2}\right)K_{14} \tag{4}$$

in which D_{14} is the diffusion coefficient for the binary mixture consisting of methanol monomers and tetramers, and ΔH_{14} is the heat of formation of tetramers according to the reaction

$$4\ CH_3OH \overset{K_{14}}{\rightleftharpoons} (CH_3OH)_4 \tag{5}$$

where K_{14} is the equilibrium constant. Differentiation of the logarithmic form of Eq. 4 with respect to 1/T yields

$$\frac{d\ \ln\ K_{14}}{d(1/T)} = \frac{d\ \ln\ A}{d(1/T)} - \frac{d\ \ln\ (pD_{14})}{d(1/T)} - 3T \tag{6}$$

The term pD_{14} may be calculated from equations developed in Hirschfelder, Curtiss and Bird:[3]

$$pD_{14} = D^{\circ}_{14} \frac{T\lambda_o}{E} \tag{7}$$

where E is the Eucken factor which corrects for the contribution of internal degrees of freedom to the thermal conductivity of polyatomic molecules, and D°_{14} is composed of essentially temperature-independent parameters. The term $d \ln (pD_{14})/d(1/T)$ lies between -621 K and -708 K for the temperature range of interest. The term $d \ln K_{14}/d(1/T)$ was evaluated from Eq. 6 at each of the five experimental temperatures; the standard enthalpy of formation of tetramer from monomer, ΔH_{14}, was then evaluated from the relationship

$$\Delta H_{14} = -R \; d \ln K_{14}/d(1/T) \tag{8}$$

in which R is the gas constant. The average value of ΔH_{14} between 306 K and 345 K was found to be -23.65 kcal/mole. This value of ΔH_{14} was used in Eq. 4 to calculate the equilibrium constant, K_{14}, at each temperature.

T(K)	K_{14} (atm^{-3})
345.14	2.190×10^{-3}
337.35	4.853×10^{-3}
326.61	1.547×10^{-2}
316.61	4.882×10^{-2}
306.89	1.610×10^{-1}

A plot of $\ln K_{14}$ *vs.* $1/T$ yields a straight line of which the slope is $\Delta H_{14}/R$ and the intercept is $\Delta S_{14}/R$. From this plot, ΔH_{14} was -23.64 kcal/mole, indicating self consistency, and ΔS_{14} was -80.7 e.u. These values may be compared with those of Weltner and Pitzer[4] who obtained -24.2 kcal/mole and -81.3 e.u. from a combination of a small number of heat capacity measurements and PVT measurements on methanol vapor.

The data sets were also fitted at all five temperatures simultaneously to an equation of the form

$$\lambda \times 10^5 = (B + CT^{1/2}) + p^3 D \exp (E/T) \tag{9}$$

where B, C, D, and E are parameters to be determined by a least squares computer method; and p, T, and λ are the experimental pressures, temperatures, and thermal conductivities, respectively.

The term $(B + CT^{1/2})$ corresponds to λ_o and $p^3 D \exp (E/T)$ corresponds to the Ap^3 term of the individual fits represented by Eq. 1. This nonlinear least squares problem was solved by using the SIMPLEX version of the Fortran subroutine STEPIT, available through the Quantum Chemistry Program Exchange (QCPE),[5] which yielded the four parameters in Eq. 9:

$$B = -14.05366913$$
$$C = 1.034891472$$
$$D = 6.080169019 \times 10^{-25}$$
$$E = 12412.59308$$

This fit of all the data simultaneously reproduces the experimental data best at the highest temperatures, where larger weighting factors were assigned to the higher pressures. Values of K_{14}, ΔH_{14} and ΔS_{14} determined from the information contained in Eq. 9 agree very well with those derived from our own single-temperature fits as well as with those of Weltner and Pitzer.

In terms of the pressure variable, the equilibrium constants, K_{1n}, for n-mer formation may be written

$$K_{1n} = p(\text{n-mer})/p^n(\text{monomer}) \tag{10}$$

and the mole fractions of the n-mers are given by

$$x(\text{n-mer}) = p(\text{n-mer})/p(\text{total}) \tag{11}$$

Since $p(\text{monomer}) \approx p(\text{total})$, then $x(\text{monomer}) \approx 1$; thus, $p(\text{tetramer}) = K_{14}p^4(\text{monomer}) \approx K_{14}p^4(\text{total})$ and $x(\text{tetramer}) \approx K_{14}p^3(\text{total})$. For each of the five temperatures studied, values of p(total) = p(saturation), p(tetramer), and x(tetramer) are presented below.

T(K)	p(total) = p(sat.), torr	p(tetramer), torr	x(tetramer)
345.14	1005	5.1	0.0051
337.35	738	3.3	0.0044
326.61	471	1.7	0.0037
316.61	302	0.93	0.0031
306.89	190	0.48	0.0025

The existence of dimers in methanol vapor is supported by PVT and heat capacity studies of several authors.[4,6] Corrections for dimers will be made but are expected to be small because thermal conductivities are most sensitive to the higher aggregates in associated vapor systems.

It is clear from our results that thermal conductivity measurements provide a sensitive means for detecting associated vapor species, especially large polymeric species. When measurements are coupled with the molecular theory of gases, one can obtain accurate values of association constants and of concentrations of polymers.

II. ELECTROMOTIVE FORCE MEASUREMENTS IN MOLTEN ALKALI METAL ALLOYS
(M. Blander)

In the development of high-energy lithium alloy/metal sulfide cells, an effort is being made to find lithium alloys that will result in improved battery performance. Thermodynamic data required for the choice of an optimum alkali metal alloy are lacking. The objectives of our study are to fill this gap and to gain insight into the basic properties of alkali metal alloys.

A. Electromotive Force Measurements in Molten Lithium-Magnesium Alloys
(M. L. Saboungi)

We report here electromotive force measurements of molten lithium-magnesium alloys using the cell:

$$\text{Li(liq, in Feltmetal)} \left| \begin{array}{c} \text{LiF-LiCl} \\ \text{(eutectic)} \\ \text{or} \\ \text{LiCl-KCl} \\ \text{(eutectic)} \end{array} \right| \begin{array}{c} \text{Li-Mg.} \\ \text{(liq)} \end{array}$$

The results of our measurements may be combined with data from the measured Li-Mg phase diagram[7] to calculate the thermodynamic properties of solid Li-Mg alloys at the solidus.

Apparatus and Procedure

The experimental arrangement of a typical cell is indicated in Fig. 6. A porous beryllia crucible contained the molten electrolyte in which was immersed the pure lithium anode. This crucible, which served as a barrier

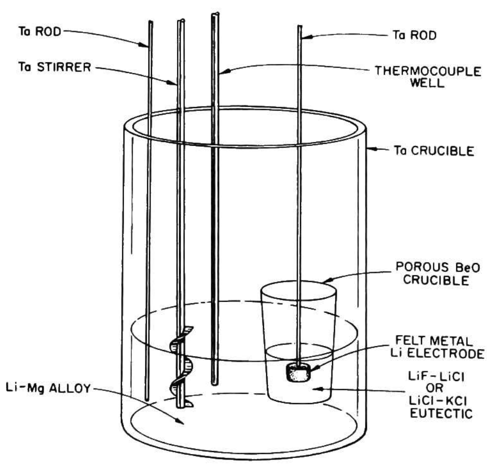

Fig. 6. Schematic of Cell for Emf Measurements.
ANL Neg. No. 308-4099 Rev. 1

to separate the two electrodes, was 20 mm in diameter and 2.4 mm in thickness; its pore size was about 50 μm. The BeO cup was pre-soaked in the molten electrolyte to wet it so as to minimize possible chemical attack by molten lithium.

The molten alloy electrode (positive electrode) was contained in a 100-mm-dia tantalum crucible. The reference electrode consisted of porous stainless steel Feltmetal (Type 347 SS) soaked in pure lithium at 500°C. At this temperature, the lithium wets the metal with such tenacity that no loss occurs when the lithium reference electrode is submerged in the electrolyte. The porosity (the pore size is about 35 μm) of the Feltmetal was quoted as being approximately 80%. Tantalum leads were used to connect both electrodes to a digital voltmeter. The entire assembly was set in a furnace well which was attached to a helium-filled glovebox. The impurities in this atmosphere consisted of 0.1 to 0.5 ppm of water while oxygen was undetected (limit of detection 1 ppm).

During each run, the temperature was constant within three degrees. The composition and temperature of the alloy were kept homogeneous by vigorous stirring with a tantalum stirrer. The emf of the cell with two pure lithium electrodes was measured first. The bias potential was always less than 0.2 mV and remained constant for several hours. The composition of the melt in the tantalum crucible was then changed by adding successive weighed amounts of magnesium. The dissolution of the magnesium in the alloy was immediate and the emf of the cell became stable (to within 0.2 mV) for as long as the composition and the temperature were held constant, often for hours and sometimes overnight. After temperature cycling, the emf generally returned to within 0.1 mV of the initial value.

The choice of electrolyte depended on the temperature of the cell. For temperatures lower than 773 K, the LiCl-KCl eutectic mixture (mp,625 K) was used. For temperatures greater than 773 K, the LiF-LiCl eutectic mixture (mp,774 K) was used in order to ensure the stability of the cell.*

The use of a large amount of alloy (40 to 50 g of lithium) appears to be significant in minimizing the effects of self-discharge, *i.e.*, the transfer of lithium from the reference electrode to the alloy.

Results and Discussion

Compositions of lithium, emf data, and activities of lithium, at four temperatures, are given in Table 1. The emf values, E, are corrected for the bias potential.

---

* At temperatures greater than 773 K, it was observed experimentally by us and by others[8] that the lithium metal reduces KCl to potassium metal, which condenses mainly on the cooler sections of the well and the electrode leads. This effect can be understood from simple thermodynamic considerations. The standard free energy of the reaction:

$$Li + KCl(\ell) \rightleftharpoons K + LiCl(\ell)$$

is about 3 kcal mol^{-1} at 800 K according to JANAF Tables.[9] Even at 723 K, the vapor pressure of potassium in this mixture is noticeable (about 1 torr).

Table 1. Emf Results at Four Temperatures

X_{Li}	E(mV)	a_{Li}	X_{Li}	E(mV)	a_{Li}
T = 670 K			T = 735 K		
0.958	2.52	0.956	0.908	6.81	0.898
0.891	6.89	0.888	0.792	16.66	0.769
0.813	13.38	0.793	0.684	30.15	0.621
0.749	19.75	0.710			
0.685	25.95	0.638			
T = 830 K			T = 887 K		
0.928	5.79	0.922	0.899	8.39	0.896
0.855	12.82	0.836	0.836	14.59	0.826
0.816	17.26	0.786	0.762	23.52	0.736
0.782	21.19	0.744	0.699	32.42	0.656
0.755	24.90	0.707	0.643	41.76	0.579
0.725	29.06	0.666	0.589	51.91	0.507
0.683	35.65	0.606	0.534	61.41	0.448
0.649	41.61	0.560	0.506	67.87	0.412
0.627	45.70	0.528	0.480	77.00	0.365
0.594	52.12	0.482	0.459	82.57	0.339
0.566	57.84	0.445	0.429	90.77	0.305
0.541	63.41	0.413	0.406	98.62	0.277
0.522	67.96	0.387	0.381	105.10	0.253
0.507	71.36	0.369	0.354	114.00	0.225
0.487	76.05	0.346	0.330	122.37	0.203
0.475	78.84	0.333	0.298	134.22	0.172

The activities of lithium in the alloys calculated from the relation

$$E = -\frac{RT}{F} \ln a_{Li} \tag{12}$$

(R is the gas constant, and F is the Faraday constant) are plotted in Fig. 7. In the molten alloys, deviations from ideality are small and negative. The activities of lithium in solid alloys at the solidus can be calculated by combining these results with the phase diagram (Fig. 8). The ratio of the activity of lithium in the molten alloy (liquid lithium is the standard state) to the activity of lithium in the solid alloy (hypothetical solid lithium is the standard state) in equilibrium with the liquid is given by

$$\ln \frac{a_{Li}}{a'_{Li}} = \frac{\Delta H_f}{R}\left(\frac{1}{T_m} - \frac{1}{T}\right) \tag{13}$$

The prime denotes solid lithium as standard state, ΔH_f is the enthalpy of fusion of lithium (0.7171 kcal mol^{-1}), and T_m is the melting point of lithium

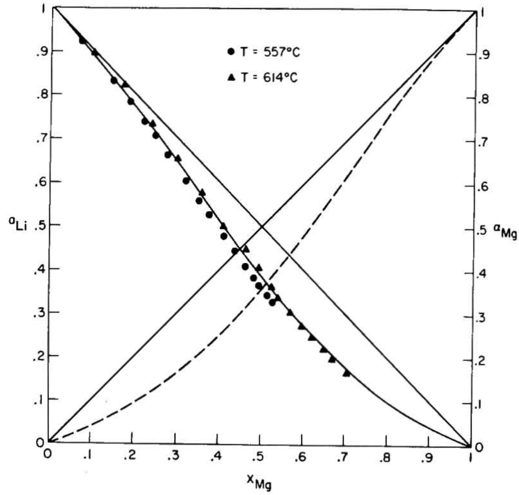

Fig. 7. Activities of Li and Mg in the Li-Mg System (● a_{Li} measured at 557°C, ▲ a_{Li} measured at 614°C, --- a_{Mg} calculated at 614°C). ANL Neg. No. 308-3952 Rev. 1

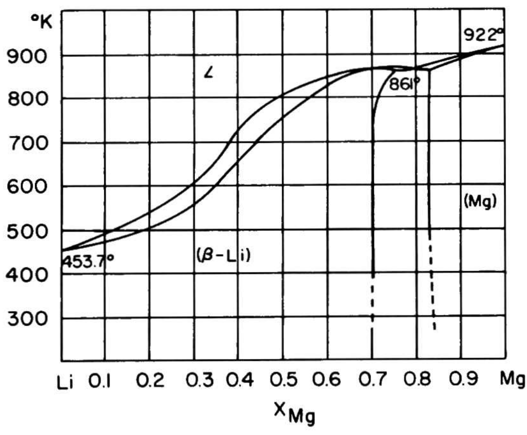

Fig. 8. Phase Diagram of the Li-Mg System.[7]
ANL Neg. No. 308-4106

(453.69 K).[9] The excess chemical potential of lithium in the molten alloys (μ^E_{Li}) is

$$\mu^E_{Li} = RT \ln \gamma_{Li} = FE - RT \ln X_{Li} \tag{14}$$

By assuming that μ^E_{Li} is independent of temperature, the activities of lithium at the liquidus may then be calculated. The composition of the solid alloy in equilibrium with the liquid is given in column 2 of Table 2. The values of the activities of solid and liquid lithium at the solidus and liquidus, respectively, at temperatures ranging from 500 K to 870 K are given in columns 3 and 4 of Table 2.

Table 2. Estimated Values of the Activity of Li[a] in Solid Li-Mg Alloys at the Solidus

T(K)	X'_{Li}	a'_{Li}	a_{Li}
500	0.80	0.80	0.87
600	0.65	0.54	0.66
700	0.56	0.40	0.53
800	0.44	0.28	0.40
850	0.36	0.18	0.27
870	0.30	0.12	0.17

[a] The concentrations, X'_{Li}, are atom fractions at the solidus. Activities in column 3 are relative to a hypothetical solid lithium as standard state and activities in column 4 are relative to liquid lithium.

As with the liquids, deviations from ideality at the solidus are relatively small and negative. At higher temperatures and lower atom fractions of lithium, activity coefficients of lithium in the solid alloy are lower than in the liquid. This is a necessary consequence of the reported maximum in the liquidus and solidus curves in the phase diagram (Fig. 8).

Table 3. Excess Chemical Potentials of Magnesium and Lithium (cal mol^{-1})

	This Work		Reference 10	
X_{Mg}	μ^E_{Li}(887 K)	μ^E_{Mg}(887 K)	μ^E_{Li}(1000 K)	μ^E_{Mg}(1000 K)
0	0	-1520	(0)	(-5800)
0.1	-6	-1430	(-78)	(-4293)
0.2	-40	-1260	-297	-3048
0.3	-110	-1030	-631	-2041
0.4	-240	-790	-1052	-1256
0.5	-440	-560	-1526	-674
0.6	-670	-360	-2004	-279
0.7	-970	-200	-2403	-61
0.8	(-1300)	(-90)	-2639	21
0.9	(-1680)	(-20)	-2602	18
1.0	(-2100)	(0)	-2192	0

( ) Extrapolated

The data at 887 K (Table 1) were utilized to calculate the activities of magnesium from the Gibbs-Duhem relation:

$$\ln \gamma_1 = -\int_{\gamma_2(0)}^{\gamma_2(X_2)} \frac{X_2}{X_1}\, d(\ln \gamma_2) = \frac{-X_2}{X_1} \ln \gamma_2(X_2) + \int_1^{X_1} \frac{\ln \gamma_2}{X_1^2}\, dX_1 \qquad (15)$$

where component 1 is Mg and component 2 is Li. The last integral was calculated using a plot of $\ln \gamma_2/X_1^2$ *vs.* X_1 which was extrapolated beyond $X_1 = 0.702$ to $X_1 = 1$. The uncertainties in the extrapolation appear to be very small. The activities of magnesium are plotted in Fig. 7. As with Li, the deviations from ideal solution behavior of Mg appear to be relatively small.

Our results for the excess chemical potentials of Li and Mg at 887 K, given in columns 2 and 3 of Table 3, respectively, differ considerably from those of Mashovets and Puchkov[7,10] at 1000 K, given in columns 4 and 5 of Table 3. Their data were derived from magnesium vapor pressure measurements at only five concentrations. The differences between our figures and theirs are too large to be ascribed only to the difference in temperature. We believe that the large asymmetry and the unusual concentration dependence of the excess chemical potentials in the studies of Mashovets and Puchkov, as well as the small number of measurements, place their results in some doubt. The small deviations from ideality of our results at all concentrations are consistent with the small difference in electronegativities and the small difference in molar volumes between Li and Mg.

We are continuing this study by carrying out measurements in the Li-Al (liquid) and in ternary lithium alloys.

III. CHEMISTRY OF MOLTEN SALTS AND THEIR VAPORS (M. Blander)

Molten salts and their vapors are important for a variety of energy-related technologies, such as batteries, fuel processing, coal gasification and coal conversion. We have continued the fundamental theoretical and experimental studies of multicomponent molten salt systems to test means of calculating their thermodynamic properties *a priori*. A knowledge of such properties is needed for battery and chemical processing technologies. We are improving our ability to make spectroscopic measurements at high temperatures in order to study, among other materials, binary salt vapor compounds and carbonium ions in acid salts. Binary salt vapor compounds have potential for chemical processing, and carbonium ions are intermediates in the catalytic conversion of coal by acidic molten salt catalysts.

A. Conformal Ionic Solution Theory for Additive Ternary Systems (M. L. Saboungi)

We have extended the conformal ionic solution (CIS)[4-13] theory up to fourth order terms for additive ternary molten systems containing three types of cations and one type of anion or three types of anions and one type of cation (AX-BX-CX or AX-AY-AZ). Fourth order terms have been shown to be necessary to adequately describe measurements of mixtures of even monovalent salts.[14,15]

1. Calculations

In the previous report,[16] calculations of the excess Helmholtz free energy of mixing ΔA_m^{XS} had been carried out up to third order:

$$\Delta A_m^{XS} = \sum_{i<j}\sum a_{ij} X_i X_j + \sum_{i\neq j}\sum b_{ij}(3)\, X_i^2 X_j + A(3)\, X_1 X_2 X_3 \tag{16}$$

The coefficient a_{ij} contains contributions from both the second and third order terms:

$$a_{ij} = a_{ij}(2) + a_{ij}(3) \tag{17}$$

The coefficient $b_{ij}(3)$ contains contributions from only the third order terms, and

$$b_{ij}(3) = -b_{ji}(3) \tag{18}$$

The ternary mixed coefficient, A(3), contains contributions from only the third order terms; and

$$A(3) = \left(b_{12}^{1/3}(3) + b_{13}^{1/3}(3)\right)\left(b_{21}^{1/3}(3) + b_{23}^{1/3}(3)\right)\left(b_{13}^{1/3}(3) + b_{23}^{1/3}(3)\right) \tag{19}$$

The calculations to fourth order proceed similarly as those to the third order. Because of its complexity, we will not describe the calculation. The result for the excess Helmholtz free energy of mixing up to fourth order is:

$$\Delta A_m^{XS} = \sum_{i<j}\sum a_{ij} X_i X_j + \sum_{i\neq j}\sum b_{ij}\, X_i^2 X_j + \sum_{i<j}\sum c_{ij} X_i^2 X_j^2$$

$$+ A\, X_1 X_2 X_3 + \sum_{\substack{i \\ i\neq j<k}}^{3} B_i X_i^2 X_j X_k \tag{20}$$

where

$$a_{ij} = a_{ij}(2) + a_{ij}(3) + a_{ij}(4) \tag{21}$$

$$b_{ij} = b_{ij}(3) + b_{ij}(4) \tag{22}$$

$$c_{ij} = c_{ij}(4) \tag{23}$$

$$A = A(3) + A(4) \tag{24}$$

and

$$B_i = B_i(4) = 2(C_{ij}C_{ik})^{1/2} \tag{25}$$

2. Evaluation of the Ternary Mixed Coefficients

The equations which we have derived can prove useful in calculating thermodynamic properties of ternary systems. Where terms up to only third order are significant, Eq. 16 applies. By allowing one of the X_i to be zero, this equation reduces to the equation for a binary system and one can evaluate the parameters a_{ij} and $b_{ij}(3)$ from measurements on the three binaries. Up to the third order, the only ternary mixed coefficient, A(3), can be calculated from the $b_{ij}(3)$, using Eq. 19. Consequently, the excess Helmholtz free energies of mixing and other thermodynamic functions of conformal ionic ternary systems may be predicted *a priori* up to the third order from data on the subsidiary binary systems.

Where terms up to fourth order are significant, Eq. 20 applies. The coefficients a_{ij}, b_{ij} and c_{ij} can be evaluated from measurements on the three binaries. The three mixed ternary coefficients B_i can be exactly calculated from the c_{ij}, using Eq. 25. The coefficient A cannot be deduced exactly from the binary data only. However, we can demonstrate that:

(1) A(4) is smaller than A(3) and, furthermore, it is small enough to neglect.

(2) A(3) can be calculated from the b_{ij} by using an equation similar to Eq. 19:

$$A \simeq A(3) \simeq \left(b_{12}^{1/3} + b_{13}^{1/3}\right)\left(b_{21}^{1/3} + b_{23}^{1/3}\right)\left(b_{13}^{1/3} + b_{23}^{1/3}\right) \tag{26}$$

where the b_{ij}'s contain contributions from both third and fourth order terms. The procedure is given elsewhere in more detail,[17] and implies a particular choice of a test salt. Thus, all terms in Eq. 20 can be evaluated *a priori* from measurements on binary subsystems.

3. Comparison with Experimental Data

The most precise measurements suitable for comparison with our calculations are measurements of the enthalpies of mixing of alkali nitrates.[14]

The data on the binary subsystems[14] used in our calculations are given in Table 4. Table 5 contains a comparison of measurements (column 4) with our calculations (column 5) in the three ternary alkali nitrate systems $(Li,Na,K)NO_3$, $(Li,Na,Rb)NO_3$ and $(Li,K,Rb)NO_3$. The differences between the calculated and measured values are generally small and about the size of the uncertainties in the measurements (about 2% of the total enthalpies of mixing but probably no less than 4 cal/mol^{-1}). Consequently, the measurements are in consonance with our calculations.

Table 4. Values[14] of the Binary Coefficients Used in the Ternary Calculations (in cal mol^{-1})

Binary System (i,j)	a_{ij}	$2b_{ij}$	c_{ij}
$(Li,Na)NO_3$	-448	-15	----
$(Li,K)NO_3$	-1659	-131	-556
$(Li,Rb)NO_3$	-2392	-204	-994
$(Na,K)NO_3$	-392	-67	----
$(Na,Rb)NO_3$	-707	-228	-236
$(K,Rb)NO_3$	-446	-33	----

4. Solutions Dilute in One Component

The total excess free energies and enthalpies of mixing are relatively insensitive to the relatively small term $AX_1X_2X_3$. However, partial molar quantities may be more sensitive and may provide an adequate test of our equations. From Eq. 20, we can calculate the activity coefficient for component 1. Simplifying to the special case of solutions infinitely dilute in component 1, we obtain the equation:

$$RT \ln \gamma_1 = a_{12}X_2 + a_{13}X_3 - a_{23}X_2X_3 - b_{12}X_2^2 - b_{13}X_3^2 + 2b_{23}X_2X_3(X_3 - X_2)$$

$$- 3c_{23}X_2^2X_3^2 + AX_2X_3 + B_2X_2^2X_3 + B_3X_2X_3^2 \qquad (27)$$

There are similar expressions for the partial molar enthalpy of solution. We may examine the relative magnitudes of the different terms in expressions for the partial molar enthalpy of solution; for the $(Li,Na,Rb)NO_3$ system, for example, where component 1 is $LiNO_3$, component 2 is $NaNO_3$ and component 3 is $RbNO_3$.

(a) Curves of $(H_1 - H_1^\circ)/(1 - X^2)$ for constant values of X_1 (X_1 = 0, 0.25, 0.50 and 0.75) plotted *vs.* $X_3/(X_3 + X_2)$ were calculated using the data from Table 5 and Eq. 26. The deviations from linearity were positive with an S-shaped character showing up as an asymmetry in the deviations for X_1 = 0, 0.25 and 0.50. For X_1 = 0.75, the S-shaped character of the curves

Table 5. Comparison of Measured[14] and Calculated Values of Molar Enthalpies of Mixing of Ternary Systems (in cal mol^{-1})

A. The $(Li,Na,K)NO_3$ System

X_{Li}	X_{Na}	X_K	ΔH^E(meas)	ΔH^E(calc)
0.0992	0.7102	0.1906	-129.4	-125.1
0.1061	0.7830	0.1109	-98.7	-97.0
0.1132	0.7048	0.1820	-131.6	-130.2
0.4866	0.2504	0.2630	-323.1	-314.4
0.4762	0.3490	0.1749	-259.4	-249.5
0.7521	0.1227	0.1252	-222.9	-219.3
0.8983	0.0530	0.0487	-102.5	-102.0
0.3826	0.2472	0.3702	-341.5	-338.3
0.2423	0.4958	0.2619	-227.0	-223.8
0.1651	0.3324	0.5025	-250.6	-241.1
0.2375	0.2521	0.5104	-306.1	-297.0
0.3197	0.1690	0.5113	-365.0	-356.1
0.3197	0.1615	0.5188	-367.0	-358.3

B. The $(Li,Na,Rb)NO_3$ System

X_{Li}	X_{Na}	X_{Rb}	ΔH^E(meas)	ΔH^E(calc)
0.2478	0.5010	0.2512	-342.1	-342.1
0.2506	0.2496	0.4998	-475.5	-479.1
0.5048	0.2516	0.2436	-452.7	-449.7
0.1244	0.7511	0.1245	-172.0	-171.0
0.7496	0.1252	0.1252	-311.7	-309.4
0.1259	0.1244	0.7497	-324.7	-328.9
0.3312	0.3346	0.3342	-456.2	-455.2
0.3299	0.3376	0.3325	-447.6	-453.0
0.2498	0.2503	0.4999	-473.4	-478.4

C. The $(Li,K,Rb)NO_3$

X_{Li}	X_K	X_{Rb}	ΔH^E(meas)	ΔH^E(calc)
0.4965	0.2520	0.2515	-580.1	-580.7
0.2496	0.4995	0.2509	-410.3	-398.5
0.2506	0.2498	0.4996	-462.0	-450.5
0.3328	0.3338	0.3334	-521.5	-509.1
0.7496	0.1249	0.1255	-430.5	-432.6
0.1251	0.7493	0.1256	-214.7	-210.0
0.1259	0.1244	0.7497	-278.1	-271.3
0.3332	0.3332	0.3336	-515.9	-509.5

is not apparent here, thus exhibiting the complexity of the solution behavior (Fig. 9). The S-shape of the curves comes from the term containing b_{23} and has been observed in some molten salt systems such as (Pb,Na,K)Cl and (Pb,Na,Cs)Cl.

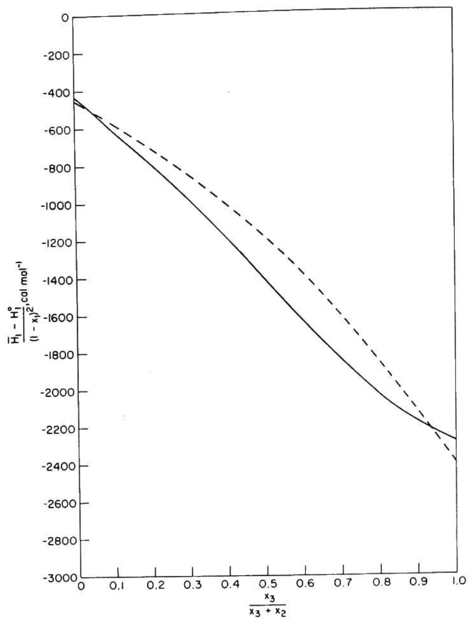

Fig. 9. Plot of $\frac{\overline{H}_1 - H_1^\circ}{(1 - X_1)^2}$ (calculated) *vs.* $\frac{X_3}{X_2 + X_3}$ at Constant Values of X_1 in the $(Li,Na,Rb)NO_3$ System (solid line: X_1 = 0; dashed line: X_1 = 0.75). ANL Neg. No. 308-3973

(b) In Fig. 10, analogous plots of $(H_2 - H_2^\circ)/(1 - X_2)^2$ *vs.* $X_3/(X_1 + X_3)$ are shown. Deviations from ideality are large and positive. They are related to the large values of the coefficient b_{13}, which is not present in any prior solution theories.

(c) A further illustration of the relatively complex behavior predicted from theory for the $LiNO_3$-$NaNO_3$-$RbNO_3$ system is shown in Figs. 11A and 11B. The terms $\overline{H}_i$, $\overline{H}_i(j)$ and $\overline{H}_i(k)$ are the partial molar enthalpies of component i, in the ternary, the binary ij and the binary ik, respectively. Figures 11A and 11B are plots of the deviations from linearity of functions such as those plotted in Figs. 9 and 10. For regular solutions (only second order terms are significant) which are usually postulated to describe such solutions this function is constant and is represented by the horizontal line. Deviations from constancy are considerable and both curves exhibit maxima which illustrate the complexity of solution behavior.

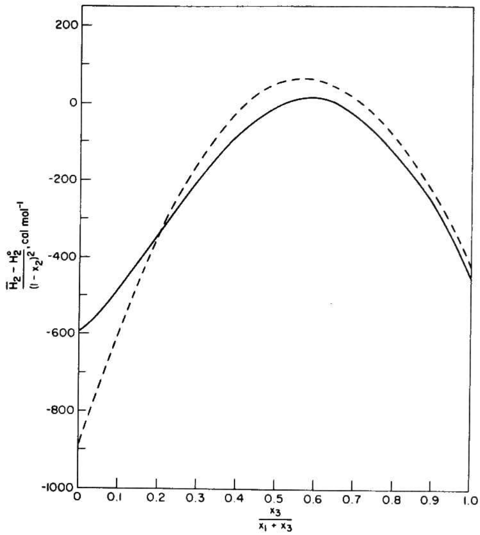

Fig. 10. Plot of $\frac{\bar{H}_2 - H_2^\circ}{(1 - X_2)^2}$ (calculated *vs.* $\frac{X_3}{X_1 + X_3}$ at Constant Values of X_2 in the (Li,Na,Rb)NO_3 System (solid line: $X_2 = 0$; dashed line: $X_2 = 0.75$). ANL Neg. No. 308-3972

5. Conclusion

The thermodynamic behavior of multicomponent additive systems is shown to be too complex to be described adequately by simple regular solution theories. It is clear that even quasi-lattice theories cannot give a reliable prediction of the properties of such systems especially when the deviations from ideal solution behavior are large. Conformal ionic solution theory provides a means of calculating *a priori* the properties of ternary systems from data on the three binary subsystems. The properties of the derived equations differ from those given in published theories, partly because of the terms in b_{ij} which lead to asymmetry in the thermodynamic properties of the binary subsystems. This difference lends a characteristic behavior to dilute solutions of one component in a binary solvent which is usually not inherent in prior theories without *ad hoc* assumptions. A comparison of theory with experimental measurements indicates that the solution behavior of ternary molten salt systems is generally complex and that detailed measurements or a reliable theory are required for a complete description and accurate predictions of the thermodynamics of solution. If a theory such as this proves to be reliable, the number of measurements required to fully analyze ternary systems can be considerably reduced. This reduction can arise for two reasons: firstly, theory provides a functional form for fitting the data; and secondly, it can give relationships between coefficients of individual terms and thus reduce the number of parameters one needs to evaluate from data.

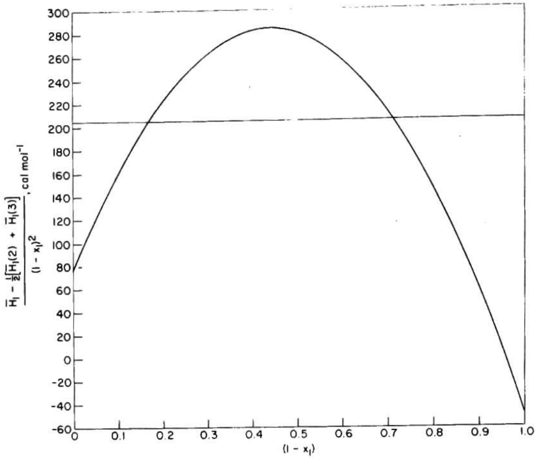

Fig. 11A. Plot of $\frac{\overline{H}_1 - \frac{1}{2}\left[\overline{H}_1(2) + \overline{H}_1(3)\right]}{(1 - X_1)^2}$ (calculated) *vs.* $(1 - X_1)$ at $X_2 = X_3$ in the (Li,Na,Rb)NO_3 System (The horizontal line represents the molar excess free energy of a 50-50 mixture of $NaNO_3$ and $RbNO_3$.) ANL Neg. No. 308-3970

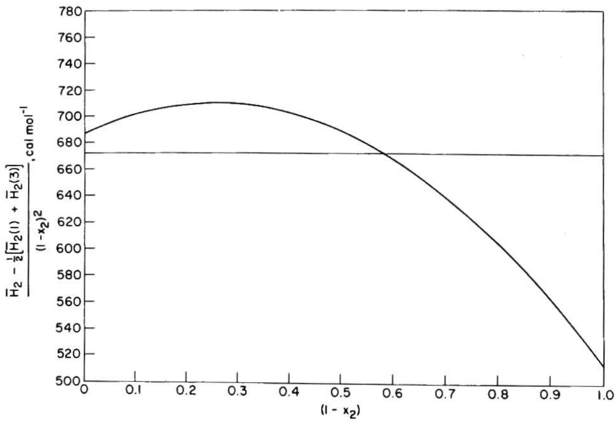

Fig. 11B. Plot of $\frac{\overline{H}_2 - \frac{1}{2}\left[\overline{H}_2(1) + \overline{H}_2(3)\right]}{(1 - X_2)^2}$ (calculated) *vs.* $(1 - X_2)$ at $X_1 = X_3$ in the (Li,Na,Rb)NO_3 System (The horizontal line represents the molar excess free energy of a 50-50 mixture of $LiNO_3$ and $RbNO_3$.) ANL Neg. No. 308-3971 Rev. 1

B. Miscibility Gaps in Reciprocal Salt Systems
(G. H. Kucera)

Predictions of liquid-liquid miscibility gaps in reciprocal molten salt systems can be made from the conformal ionic solution (CIS) theory. These predictions have been tested for only one system and indicate the validity of the theory for temperatures not too far below the upper consolute temperature.[18] A test of the theory at temperatures far below the consolute temperature is necessary in order to better define the range of validity of the predictions.

Measurements of the miscibility gap in the ternary reciprocal salt system Na,Ag||NO_3,Br can provide such a test. The visual, titration technique described previously[19] was used to acquire further experimental data. A pot furnace, controlled by a variac, was used to heat a 300-ml fused silica open beaker containing a vigorously stirred solution. Weighed additions of solutes (*e.g.*, $AgNO_3$ or NaBr) were made to ∿1 mole of $NaNO_3$ until the color of a tiny drop of a second phase was observed. The temperature was monitored with a calibrated Pt-Pt/10% Rh thermocouple immersed in the melt. The instability of $AgNO_3$ at the experimental temperatures limited the measurements to those regions where the activity of the $AgNO_3$ was low; hence, only the upper boundary of an isotherm could be located. The data for the 540°C isotherm are shown in Fig. 12 and are represented by the solid line and symbols.

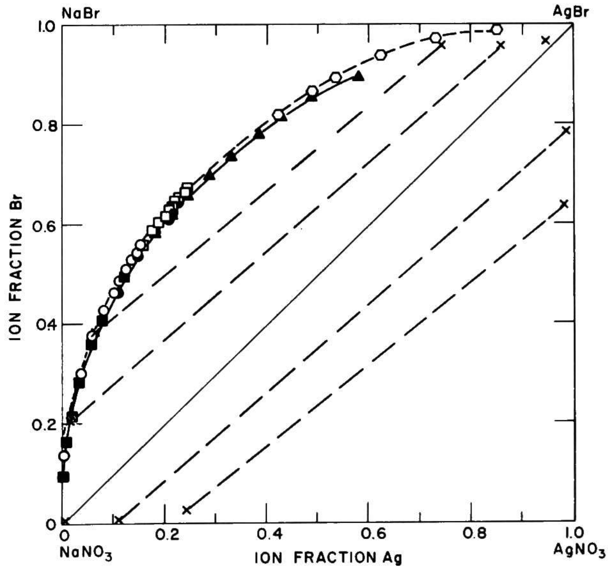

Fig. 12. Experimental Miscibility-Gap Isotherms in the Reciprocal Molten Salt System Na,Ag||NO_3,Br

The dashed line and open symbols show the data previously collected at 520°C. Each set of symbols on the individual curves indicates a single run. It is apparent from the points on the 540°C isotherm that the reproducibility of a single point or of a segment of the miscibility gap boundary is very good. In general, the isotherms were measured to within 0.5 mol %.

To further define an equilibrium isotherm in the miscibility gap, tie line data were obtained for five different pairs of immiscible liquids equilibrated at 520°C and analyzed chemically. The compositions of these pairs are plotted in Fig. 12 and are indicated by X's connected by dashed lines. These tie lines are asymmetric, consistent with expectations from theory.

A preliminary analysis indicates that our experimental results are consistent with predictions from the CIS theory at temperatures far below the estimated upper consolute temperature of 1700°C. As predicted, the temperature dependence of the miscibility gap is small and the size of the gap is in accord with our calculations and with a previous finding that the parameter Z in the theory should be 6.[18] Thus, the choice of this value of Z appears to be adequate for the description of a broad range of systems. Detailed theoretical calculations are in progress.

C. Salt Vapor Studies
(G. N. Papatheodorou)

It is known that the volatility of many inorganic salts (*e.g.*, the halide salts of alkali metals,[20] transition metals,[20,21] lanthanides,[22] and actinides[23]) is enhanced by the presence of "acidic gases" such as $AlCl_3$ and $FeCl_3$, owing to the formation of gaseous complexes. In some cases,[21] the enhancement of volatility reaches factors up to 10^{10}, suggesting that the gaseous complexes might be useful for crystal growth, rapid chemical transport, and separation of mixtures of inorganic salts by vapor processes. A planned systematic investigation of the thermodynamics of vaporization and of the structure of these gaseous complexes includes Raman spectroscopic, electronic absorption spectroscopic and transpiration studies. In the following paragraphs new optics in the laser Raman system and a new furnace necessary for spectroscopic studies of vapors are briefly described.

1. New Optics. Figure 13 shows the new optics of the laser Raman spectroscopy system designed for use at high temperature.

An emission line of the argon laser is first isolated from the ultraviolet plasma radiation by passing through two Pellin-Brocca (constant deviation) prisms. The laser beam is then reflected on two front surface adjustable mirrors, passes through a half-wave plate and illuminates the sample in the furnace. A microscope objective lens on an x-y-z micropositioner is used for accurate focusing of the laser on the sample. For collecting the scattered radiation, an f:1 50 mm CaF_2 lens is used on another x-y-z micropositioner. The image of the scattered radiation is rotated, so as to be parallel to the slit of the monochromator, with the aid of a dove prism and then is passed through a polarizer. Finally, the radiation is analyzed with a Spex 1400 double monochromator equipped with a photomultiplier tube.

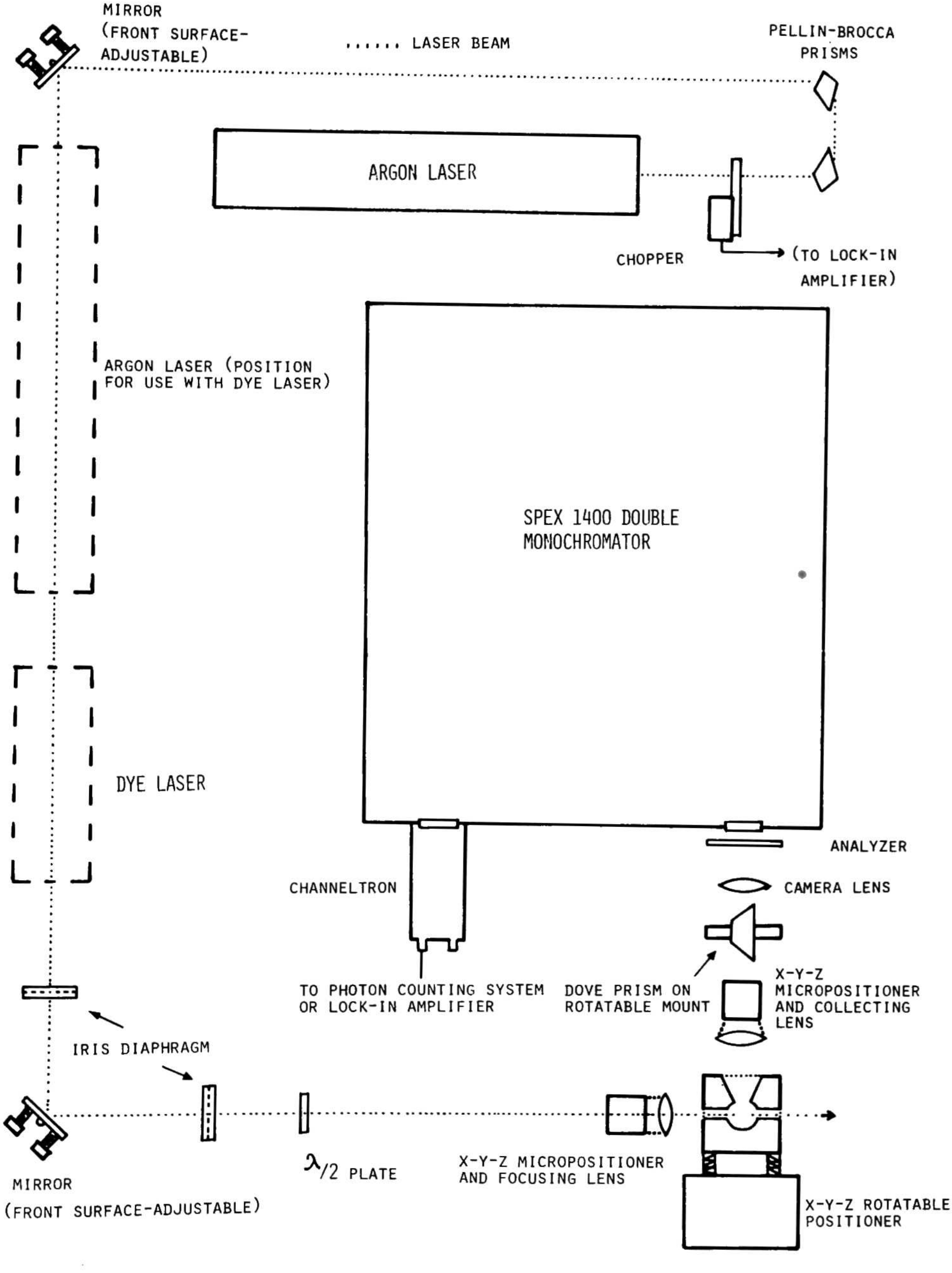

Fig. 13. Apparatus and Collection Optics for Laser Raman Spectroscopy

2. The Furnace. A schematic of the optical furnace is shown in Fig. 14. The main heater block is made of Inconel tubing, grooved and

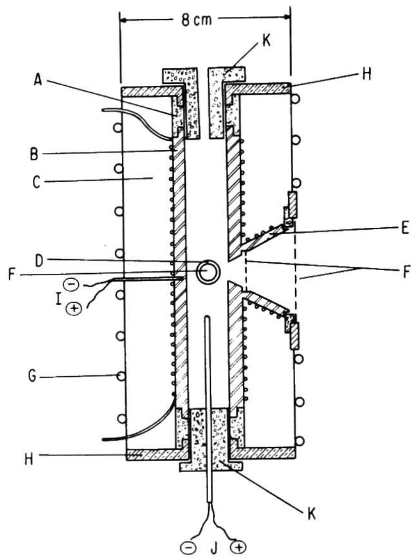

Fig. 14. Furnace for High-Temperature Raman Spectroscopy

A: Lavite Rings
B: Main Inconel Heater
C: Bubble Alumina Insulation
D: Inconel Tube Opening
E: Inconel Conical Opening
F: Fused Silica Windows
G: Water Cooling
H: Brass Supports
I: Controlling Thermocouple
J: Thermocouple for Measuring and Adjusting Temperature Gradients
K: Lavite Plugs
L: Fused Silica Cylindrical Cell
M: Fused Silica Rod

wound with sheathed nichrome cable. The laser beam passes through an Inconel tube opening (D) perpendicular to the main heater and the scattered radiation is collected at right angle to the incident beam through an Inconel conical opening (E). Both openings (E and D) are also grooved and wound with a separate sheathed nichrome cable. Fused silica windows are attached to the outer jacket so as to cover the optical openings. The copper outer jacket is water cooled via copper tubing soldered in place and the intervening space between the heater and the jacket is insulated with bubble alumina. The temperature gradients in the furnace are adjusted by using two separate power supplies so that the current through the main and central heaters can be varied independently as a function of temperature, according to prior calibration. The central heater power supply is actuated by a temperature controller.

Preliminary measurements on vapors at high temperatures indicate that the system has a sensitivity adequate for the study of salt vapors.

IV. PHYSICAL CHEMISTRY OF ALKALI METAL-SULFIDE BATTERY SYSTEMS
(R. K. Steunenberg)

High-temperature batteries that are currently under development at Argonne National Laboratory for electric automobiles and for load leveling in electric utility systems use a solid lithium-aluminum alloy for the negative electrodes, iron sulfide (FeS or FeS_2) for the positive electrodes, and molten LiCl-KCl eutectic (m.p. 352°C) for the electrolyte.[24] Two basic research studies have been conducted in connection with these batteries. One consisted of investigations of the phases formed in the iron sulfide electrodes as they are charged and discharged, and the effects of the addition of other metal sulfides on those phases. In the other study, the emfs of lithium-alloys *vs.* lithium were measured to determine the activity of lithium in the lithium-rich region of the lithium-aluminum phase diagram, and to verify the location of liquidus curves in that part of the diagram. A brief, supplemental study was also conducted on the free energy of Li_2C_2 formation by emf methods.

A. Phase Studies of Iron Sulfide Electrodes
(A. E. Martin)

1. The Li-Fe-S System at 400°C

In earlier investigations of the Li-Fe-S system conducted in the battery development program,[25] two intermediate compounds having the tentative compositions Li_2FeS_2 and $Li_4Fe_2S_5$ were identified in partially charged or discharged FeS_2 electrodes. The objective of the present study was to develop a fuller understanding of the ternary phase diagram, Li-Fe-S, at 400°C, which is in the temperature range of interest for battery operation. The original plan was to apply electron microprobe techniques in an experimental investigation of the system, but the necessary inert-atmosphere metallographic facilities for this work were not completed. However, a literature search of phase data on the Li-Fe-S system yielded useful results.

Only two stable iron sulfides, $Fe_{1-x}S$ and FeS_2, are reported to exist at 400°C. Iron disulfide (FeS_2) is essentially a line compound. The composition of $Fe_{1-x}S$, however, can vary from $Fe_{0.89}S$ to FeS at 400°C, and the exact composition (for example, the "FeS" phase formed in the sulfide electrode of a cell at 400°C) can be determined from a measurement of the lattice parameter of a quenched sample.[26] The equilibrium vapor pressure of sulfur over $Fe_{0.89}S$ is more than a thousandfold greater than that over FeS.[27]

The search also indicated that no compounds are formed between lithium and iron at 400°C,[28] and that only one compound, Li_2S, is formed between lithium and sulfur.[29] The sulfur-rich portion of the condensed Li-S phase diagram[29] at modest temperatures (above about 300°C) is similar to that of the condensed Fe-S phase diagram[30] at higher temperatures (above about 1000°C). In each diagram, a liquid miscibility gap exists between an essentially pure liquid sulfur phase, L_1, and a second liquid phase, L_2. In the Li-S system, the composition of the L_2 phase is $Li_{0.59}S$ at 400°C, and in the Fe-S system it is $Fe_{0.55}S$ at 1092°C. Because of the similarity in the form of these two diagrams and in the compositions of the L_2 liquid phases, one can infer that in the ternary Li-Fe-S system at high pressures a continuous liquid field exists between the two L_2 liquids. At a typical cell operating temperature of 400°C, however, the L_2 liquid field would extend only partially into the ternary system, from the Li-S binary in the direction of the $Fe_{0.55}S$ composition of the Fe-S binary system. However, in a practical cell system, the composition of the active material in the sulfide electrode would reach this liquid region of the Li-Fe-S phase diagram only if a large amount of Li_2S were added to the electrode. (This has been done in some experimental cells.)

As indicated above, the earlier study of the Li-Fe-S system had indicated the existence of only two ternary phases in the system; these were initially designated as the X and Z phases. The X phase was identified as Li_2FeS_2; the Z phase has the approximate composition, $Li_4Fe_2S_5$. A subsequent reexamination of samples from that study by metallographic methods showed the existence of an additional phase, Y, which was difficult to distinguish from the Z phase because both have compositions near $Li_4Fe_2S_5$. When an inert-atmosphere metallographic facility is available, it may be possible to establish the compositions of the Y and Z phases by electron-microprobe studies of existing preparations of these materials. The X and Z phases have been observed routinely in the sulfide electrodes of Li/FeS_2 cells. The Y phase, on the other hand, has been observed only in samples prepared by chemical synthesis. Because the Y phase has a higher sulfur content than the X or Z phases, however, it might be formed in the sulfide electrodes of Li/Fe_2S cells to which Li_2S has been added.

2. The Li-Cu-Fe-S System at 400°C

Copper sulfide (Cu_2S) is one of the various metal sulfides that have been added to FeS and FeS_2 electrodes to improve cell performance. Selected portions of the Li-Cu-Fe-S system were investigated as an aid to the understanding of the effect of Cu_2S additions on the reactions that occur in the iron sulfide electrodes.

The possibility of compound formation between Li_2S and Cu_2S was studied by heating pelletized mixtures of the two powders and examining the products by metallography and X-ray diffraction.* Pellets having Li_2S:Cu_2S mole ratios of 75-25, 60-40, 50-50, 40-60, 25-75 and 20-80 were

*All X-ray diffraction results reported in this section were obtained by B. S. Tani of the Analytical Chemistry Laboratory, Chemical Engineering Division.

heated at various temperatures and then annealed at 400°C. The X-ray results indicated that two or possibly three compounds had formed. One of these compounds had been observed earlier in the sulfide electrode of a Li/Cu_2S cell. The X-ray data were not definitive enough to indicate the composition of the compounds, but they did indicate that Cu_2S is significantly soluble in Li_2S at 400°C. The Li_2S-Cu_2S product with a mole ratio of 75:25 was essentially Li_2S with dissolved Cu_2S; the lattice parameter was 5.662 Å instead of the normal value of 5.712 Å.

Several Li_2S-FeS-Cu_2S preparations were made to verify earlier evidence from Li/FeS-Cu_2S cells that Cu_2S is soluble to a considerable degree in Li_2FeS_2. Metallographic examinations of the Li_2FeS_2 phase in the sulfide electrodes of such cells had shown that the phase was more anisotropic than normal, and X-ray diffraction data had shown that the lattice parameters were modified. Accordingly, preparations were made at selected compositions along the Cu_2S-Li_2FeS_2 join in the Li_2S-FeS-Cu_2S system, namely, at Cu_2S concentrations of 11, 15, 20, and 30 mol %. In each sample, the major phase was Li_2FeS_2 with modified lattice parameters that were similar to those observed in material from the electrodes. The maximum shift in the lattice parameter was observed at 20 mol % Cu_2S, which appears to be the solubility limit of Cu_2S in Li_2S. In the samples containing 11, 15, and 20 mol % Cu_2S, the second phase was Li_2S; in the sample containing 30 mol % Cu_2S, the second phase was one of the Li_2S-Cu_2S compounds.

3. The Li-Co-Fe-S System at 400°C

Cobalt sulfides have also been used as additives to the sulfide electrodes of Li/FeS and Li/FeS_2 cells to obtain improved electrical performance. Consequently, selected regions of the Li-Co-Fe-S system at 400°C were investigated to obtain additional insight into the effects of cobalt sulfide additions on the sulfide electrode reactions.

The three cobalt sulfides that were available for this study were labeled by the suppliers as CoS, Co_2S_3, and CoS_2. However, the Co-S phase diagram[5] indicates that of the three sulfides, only CoS_2 is stable at 400°C; CoS is unstable below 460°C and Co_2S_3 does not exist as a stable phase at any temperature. At a cell temperature of 400°C, the CoS material would actually be present as Co_9S_8 plus a minor amount of Co_3S_4, and the Co_2S_3 as a mixture of Co_9S_8 and Co_3S_4.

Mixtures of Li_2S with each of the three cobalt sulfides were pressed into pellets and heated as follows: Li_2S-CoS for 19 days at 400°C, Li_2S-Co_2S_3 for 1 hr at 950°C and then for 0.5 hr at 400°C, and Li_2S-CoS_2 for 16 hr at 620°C and then for 16 hr at 400°C. Metallographic examination of the products indicated that no reactions had occurred, and X-ray diffraction data confirmed the conclusion that no compounds had formed. Furthermore, in each case the Li_2S phase had its normal lattice parameter. These results indicate that there is no significant solubility of the cobalt sulfides in Li_2S at 400°C.

An additional experiment was performed in which pellets of Li_2S, CoS, and FeS in a mole ratio of 50:10:40 were heated for 1 hr at 950°C and then for 0.5 hr at 400°C. Metallographic and X-ray examinations showed that Li_2FeS_2, with its normal lattice parameter, was the major phase in the product; hence, CoS does not appear to be significantly soluble in Li_2FeS_2 at 400°C.

4. Formation of the "J" Phase

A material that is basically a Li-K-Fe-S phase (designated as J phase) has been found in partially charged or discharged sulfide electrodes of Li/LiCl-KCl/FeS cells. The KCl in the electrolyte obviously participates in the formation of the J phase, since the electrolyte is the only source of potassium in this cell system. On the basis of chemical analyses of J phase recovered from engineering-scale cells, its composition has been estimated as $K_{2.8}Li_{0.4}Fe_{12}S_{13}$.[31] (Although X-ray results showed only J phase in this material, metallographic examination indicated the presence of iron as a minor phase.) It has been noted[32] that the X-ray diffraction powder pattern of the J phase and its composition are similar to those of the mineral, djerfisherite. This mineral was first identified in meteorites, but was subsequently also found terrestially.[33] Attempts to synthesize djerfisherite as a single-phase material have been unsuccessful.[33]

The possibility of forming the J phase by out-of-cell reactions was investigated with the objective of obtaining a higher purity material than that recovered from cells, so that the composition and stability of the J phase could be determined more exactly. The first indication that the J phase could be formed by an out-of-cell chemical reaction was when it was observed as a by-product in the synthesis of Li_2FeS_2 through the reaction of Li_2S, FeS_2, and iron powders in molten LiCl-KCl eutectic (58.4 mol % LiCl-41.8 mol % KCl) at 400°C. The reaction of a similar mixture of powders in the absence of LiCl-KCl produced no J phase. The J phase has also been formed by the reaction of FeS and K_2S (sulfurated potash, Fisher P-307) for two days in LiCl-KCl eutectic at 400°C. In this case, the J phase formed as layers on the FeS particles. However, further efforts to duplicate or improve this method of synthesis were not successful.

More recently, a method has been devised for preparing the J phase by reacting Li_2FeS_2 with iron in molten LiCl-KCl and isolating it in essentially pure form. In this method, all of the constituents of the sample, other than the J phase and iron, are water-soluble and can be removed by leaching; the excess iron can then be removed either magnetically or mechanically. The first step in the procedure was the preparation of the Li_2FeS_2 reactant by the direct reaction of Li_2S and FeS in a mole ratio of 54:46; this ratio allowed for the volatilization of impurities from the Li_2S and ensured a slight excess of Li_2S, rather than FeS, in the product. This procedure facilitates later purification of the J phase because Li_2S is water-soluble, whereas FeS is not. The Li_2S-FeS mixture was melted in a graphite crucible at about 1200°C; the melt was then cooled to about 850°C and held at that temperature for 3 hr to promote the complete formation of Li_2FeS_2, which is the only known compound in the Li_2S-FeS system. The peritectic decomposition temperature of Li_2FeS_2 is about 885°C. Examination of the product showed Li_2FeS_2 as the major phase and Li_2S as a minor phase.

The Li_2FeS_2-Li_2S was ground to a powder, mixed with powdered LiCl-KCl eutectic, and reacted with excess iron at about 400°C. Initially, the iron was added in the form of a powder and the excess was removed magnetically, but the removal was not complete. In later experiments, the iron was added as wire or thin sheet, and the reaction product could be crushed to free the wire or sheet, which could then be completely removed mechanically prior to the hydrolysis treatment. Results of X-ray diffraction on a sample of J phase prepared by the iron-wire method showed it to be a single-phase material. Larger quantities of J phase material are being prepared using iron sheet so that the composition of J phase can be determined more exactly.

The effect of temperature on the formation of J phase was studied briefly. In initial short-term (1-2 hr) experiments above 500°C, no J phase product was obtained. Three-day experiments were then performed at temperatures of 402, 497, and 585°C. Metallographic examination of the products showed that at 402°C the Li_2FeS_2 particles had reacted completely to form J phase and Li_2S, but at 585°C no detectable reaction had occurred. At 497°C the extent of the reaction was so slight that it might have occurred during cooling. Thus, it appears that the reaction does not occur above 500°C.

B. Emf Studies of Lithium-Aluminum Alloys
(J. R. Selman, C. J. Cajigas)

The use of liquid lithium in the negative electrodes of high-temperature batteries being developed in this laboratory has been discontinued because of its corrosivity toward ceramics, its solubility in the molten LiCl-KCl electrolyte, and its loss of capability to wet porous metal substrate materials upon repeated charge-discharge cycling. To alleviate these problems, a solid lithium-aluminum alloy (β-phase LiAl, 50 at. % Li) is now being used as the active material in the negative electrode. At 425°C the β phase has a potential of +0.3 V relative to liquid lithium metal, and a corresponding lithium activity of 0.007. However, the specific energy of β-phase electrodes is much less than that of liquid lithium electrodes, and an alloy of higher lithium content would be desirable provided that the activity was relatively low (*e.g.*, ∿0.1) and that the alloy was a solid at the cell operating temperatures.

Since no information is available on the activity of lithium in the lithium-rich half of the Li-Al phase diagram, an emf study of this region has been undertaken. This study was also expected to yield information about the liquid-phase boundaries in this half of the diagram, which are apparently not well-defined, and on the stoichiometry of solid lithium-rich compounds. Recent publications[34,35] have cast doubt on the existence of the compound Li_2Al which is listed in standard compilations;[28] the more recent literature indicates, instead, the existence, at room temperature, of the compounds Li_3Al_2 and Li_9Al_4.

The emf measurements were made on cells of the type

$$Li/electrolyte/Li_xAl_{1-x}$$

where the electrolyte is the LiCl-KCl eutectic or another molten-halide eutectic salt containing only lithium cations. Samples of the lithium-aluminum alloy were prepared by heating the metals together at 750-800°C and absorbing the liquid in porous stainless steel plaques, followed by annealing for 48 hours at 500°C. To perform the emf measurement, a plaque was immersed in a small porous BeO crucible containing the molten-salt electrolyte, and the crucible was immersed in a pool of lithium metal, which served as the reference electrode.

The emf of a sample was measured at constant composition and varying temperature. Figure 15 shows the lithium activities corresponding to the emf measurements made on a sample containing 69.3 at. % lithium at temperatures

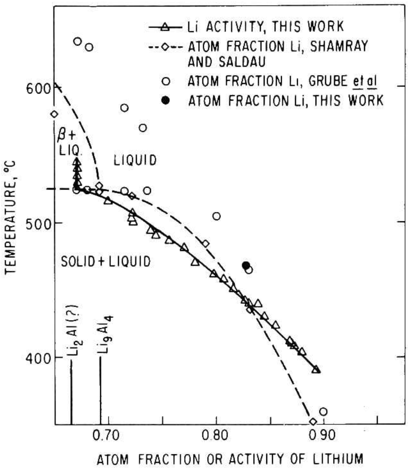

Fig. 15.

Lithium Activities for Li-30.7 at. % Al Alloy Compared with Liquidus Compositions in the Li-Al Phase Diagram

between 390°C and 550°C. A change in the slope of the curve at 522°C confirms the existence of a phase transition at this temperature, as indicated by Hansen.[28] The lithium activity values are compared in Fig. 15 with the liquidus compositions reported in the literature.[36,37] Although the liquidus data from the two sources are discrepant, the activities are close to the liquidus compositions; therefore, the sample composition is within a solid-liquid two-phase region. Similar results from samples containing 62.8 and 80.3 at. % lithium indicated that this region is wider than is shown in the phase diagram[28] and proved that the compounds Li_9Al_4 and Li_2Al do not exist in in the temperature range 390-550°C.

Figure 16 shows the results of emf measurements at 427°C (700 K) for samples of various compositions. The β-phase boundary has been sketched in from the results of a concurrent investigation of this system by differential thermal analysis.[38] The emfs for the α + β two-phase region and for two compositions in the β region are extrapolated from data of Yao *et al.*[39] The potential difference between the alloy and liquid lithium, which is 296 mV in the (α + β) two-phase region, decreases steeply in the composition range from 46 to 55 at. % lithium (in the single β-phase region). These results indicate that the use of lithium-aluminum electrodes containing more than 50 at. % lithium is not feasible in practical cells because of the high

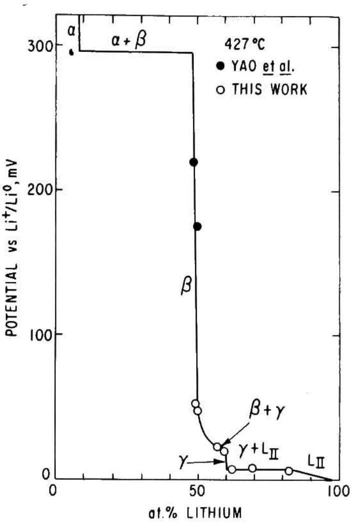

Fig. 16.

Emf-Composition Diagram for Lithium-Aluminum Alloys at 427°C (700 K)

lithium activity at these concentrations. Moreover, the solid-liquid two-phase region apparently extends from the compound Li_3Al_2 to the lithium-rich liquidus; the maximum lithium concentration in solid alloys is therefore 60 at. %.

The steep increase of the lithium activity in the β phase is accompanied by a reversal of the temperature dependence of the emf on going from the (α + β) two-phase region to the (Li_3Al_2 + liquid) two-phase region, as shown in Fig. 17.

To determine the lithium-rich liquidus more accurately, coulometric emf measurements have been made by discharging lithium from alloy samples containing approximately 90 at. % lithium. In these measurements the earlier cell arrangement was reversed, that is, the porous BeO crucible, containing the electrolyte and the lithium reference electrode, was immersed in the liquid alloy sample. The reference electrode was a porous metal plaque saturated with lithium. Only with a large amount of alloy sample was the long-term stability of the emf satisfactory. At 470°C the liquidus was found at 82.8 ± 0.3 at. % (Fig. 18). This value, which is also plotted in Fig. 15, agrees more closely with the data of Grube *et al.*[37] than with those of Shamray and Saldau[12] (80 at. % at 470°C), which were adopted by Hansen.[28] The lithium activity coefficient was 0.94, which is in agreement with a negative deviation from ideality recently reported[40] for the entire composition range at temperatures between 630 and 820°C. Coulometric emf measurements are being continued at temperatures of 400, 510, and 550°C.

C. Electrochemistry of Lithium Carbide
(J. R. Selman)

Work on the electrochemistry of lithium carbide was prompted by an apparent lithium-carbon interaction in molten LiCl-KCl eutectic electrolyte

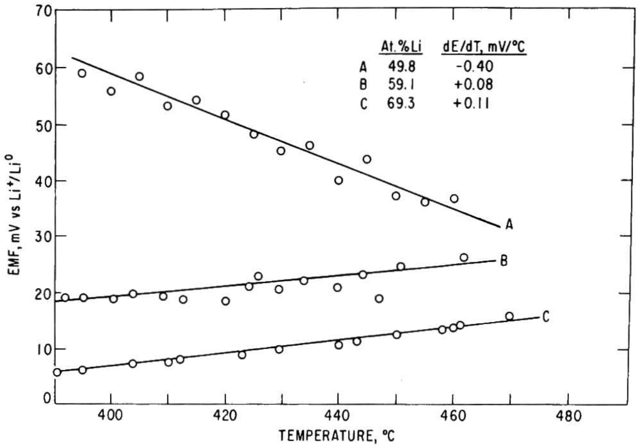

Fig. 17. Temperature Dependence of the Emf for Alloy Compositions in Three Different Regions of the Li-Al Phase Diagram

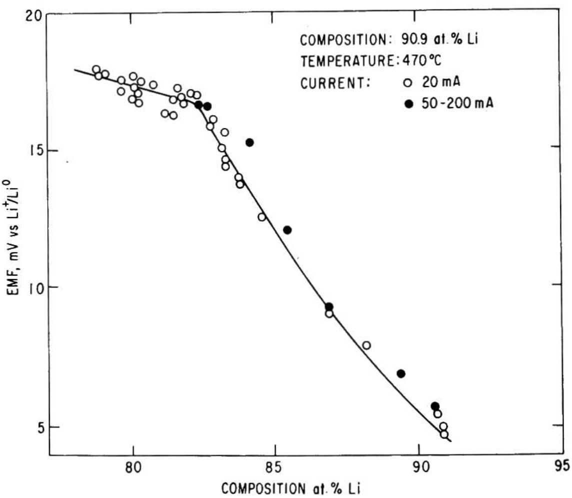

Fig. 18. Coulometric Emf Measurement of the Lithium-Rich Liquidus at 470°C

that had been observed during the overdischarge of lithium/sulfide cells with porous graphite current collectors in the positive electrodes, and also in various basic research studies in which carbon electrodes were used. The possibility that carbide might be formed in this interaction made it desirable to investigate the electrochemistry of carbide in molten LiCl-KCl eutectic. The experiments described here are considered to be exploratory, because the commercially available Li_2C_2* that was used contained substantial amounts of metallic lithium, elemental carbon, and Li_2O, which may affect the behavior of carbide in solution.

The potentials of spectrographic-grade graphite immersed in molten LiCl-KCl eutectic saturated with Li_2C_2 were measured at various temperatures. The original measurements were made *vs.* a liquid lithium electrode, but this procedure was not satisfactory because of rather rapid self-discharge of the cell. Subsequent measurements *vs.* a Li-Al reference electrode (in the two-phase $\alpha + \beta$ region of the system) gave stable potentials over periods of several hours.

The potentials that were measured in this manner were fairly reproducible ($\pm$50 mV); these are shown, relative to the potential of liquid lithium, in Fig. 19. These potentials would yield the standard free energy of formation of Li_2C_2 at the various temperatures provided that the following reaction occurs reversibly at the positive electrode:

$$2\,C + 2\,e \rightleftarrows C_2^{=} \tag{28}$$

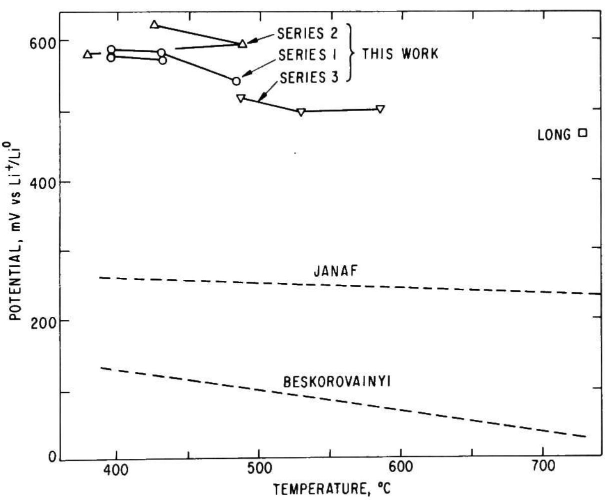

Fig. 19. Potentials of Graphite in Molten LiCl-KCl Saturated with Li_2C_2

* Alfa Products, Ventron Corp., Beverly, Mass. 01915.

Values for ΔG_f° found in the literature[41-43] show sizable discrepancies (see Table 6; also Fig. 19). The present data suggest that the free energy of formation of Li_2C_2 is approximately -26 kcal/mol at 700 K. However, there is as yet no evidence that Reaction 28 is reversible; therefore, the observed potential cannot be ascribed unambiguously to Li_2C_2 formation.

Table 6. Values for ΔG_f° of Li_2C_2 (kcal/mol)

	298 K	700 K	1000 K
JANAF[41]	-13.41	-11.92	-10.71
Beskorovainyi *et al.*[42] (estimate)	-10.86	- 5.7	- 1.4
Long[43]			-21.5
This Work[a]		-26	

[a] Tentative value owing to uncertainty in the reversibility of the cell reaction (see text).

Reaction 28 was explored subsequently by cyclic voltammetry. Figure 20 shows a voltammogram obtained at a graphite electrode in LiCl-KCl in the absence of Li_2C_2; Fig. 21 was obtained after the addition of sufficient Li_2C_2

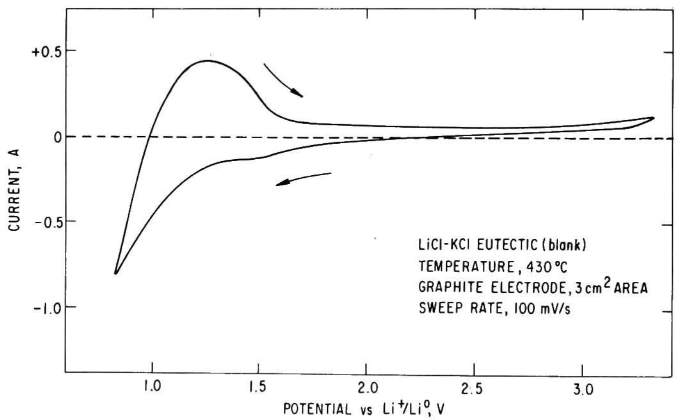

Fig. 20. Cyclic Voltammogram of a Graphite Electrode in Molten LiCl-KCl Eutectic

to give a concentration of 0.05 M. The current surge at +1 V *vs.* Li+/Li°, which results from an undefined interaction with graphite, and the subsequent oxidation peak were unchanged by the addition of Li_2C_2. However, an oxidation peak occurred at +2.8 V, which decayed in time but reappeared when more

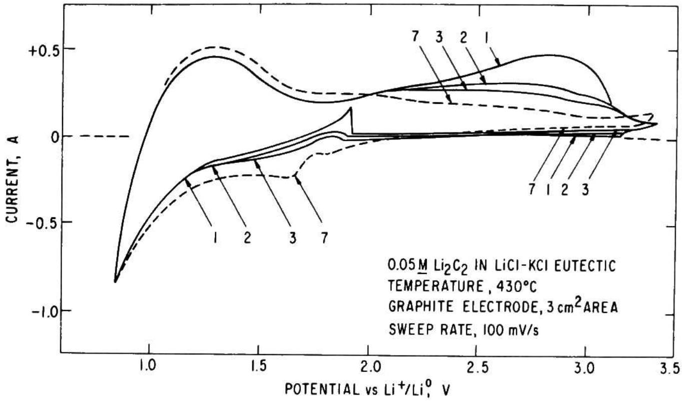

Fig. 21. Cyclic Voltammogram of a Graphite Electrode in Molten LiCl-KCl Eutectic Saturated with Li_2C_2 (The numbers indicate successive cycles.)

Li_2C_2 was added. Oxidation of $C_2^{=}$ ions apparently takes place at +2.8 V, a potential that is unexpectedly high and is very close to the potential for $O^{=}$ ion oxidation in LiCl-KCl. The reduction maxima at +1.7 V probably do not result from carbon reduction but rather from the reduction of adsorbed oxygen.

Confirmation of the apparent oxidation potential for $C_2^{=}$ ions is being sought by chronopotentiometry.

V. METEORITIC STUDIES
(M. Blander)

The theoretical and experimental studies of meteorites are aimed at understanding the origins of chondritic meteorites and chemical processes in the early solar system. The concepts under examination arise from the constrained equilibrium theory, which leads to predictions of the chemistry and petrographic properties of meteorites and the precursors of planets.

A. Supercooling of Laser-Melted Silicates: Application to the Formation of Meteorites
(M. Blander, G. H. Kucera, H. N. Planner,* K. Keil,* L. S. Nelson,** and N. L. Richardson**)

1. Introduction

Chondrules are millimeter-sized spherical bodies found embedded in the matrix of the largest class of meteorites, the chondrites. They appear

---

* University of New Mexico, Alburquerque, New Mexico 87131

** Sandia Laboratories, Albuquerque, New Mexico 87115.

to have been molten silicate droplets which crystallized rapidly. Since chondrites crystallized 4.6 billion years ago, an understanding of the mode of formation of chondrules can provide clues on the ancient origins of meteorites and, presumably, on the early history of the solar system. This experimental study of the crystallization of metastable supercooled liquid Mg_2SiO_4-SiO_2 mixtures was carried out in order to understand the conditions under which chondrules may have formed, and to better understand the behavior of supercooled liquids. A preliminary report was made previously.[44]

2. Laser-Melting

A CO_2 laser was used to melt enstatite ($MgSiO_3$) onto loops of iridium wire to form 1.0-2.6 mm beads. Each bead was then supported in a furnace held at temperatures ranging from 970 to 1346°C and was remelted by the focused beam of the laser.

During the melting, some silica vaporized, changing compositions. The laser was turned off and the molten beads cooled to temperatures which were close to the furnace temperatures and about 400-750°C below liquidus temperatures. These metastable supercooled droplets crystallized with the characteristic brightening or recalescence which comes from the temperature rise caused by the release of the enthalpy of fusion. Some of the spherules which had formed a glass were devitrified in a furnace at temperatures of 800-924°C.

3. Sectioning and Analysis

Polished thin sections were made from each of the spherules for examination by optical microscopy and the electron microprobe. Broad beam microprobe analyses indicated that the bulk compositions of the spherules varied from 44 to 56 wt % SiO_2, indicating varying loss of silica from the original 60 wt % SiO_2. The only crystalline material detected with X-rays was forsterite (Mg_2SiO_4), and the residual amorphous material was undoubtedly a glass. In 7 of the 49 spherules where the composition of the residual glass could be measured, the SiO_2 content was 65 wt %.

From the size of the spherules, the cooling times, and the furnace temperatures, the temperature of the spherules at the time crystallization began was estimated to range from 985 to 1346°C.

4. Internal Features and Nucleation Temperatures

Microscopic examination of the thin sections indicated different crystal morphologies ranging from skeletal bars, dendrites, and fibers to those classed as submicroscopic. With increasing supercooling for given compositions, the crystal morphology changed from bar + dendrite to dendrite + fiber to fiber + submicroscopic associations. Crystal sizes tended to decrease from >2 μm to <0.3 μm with increasing supercooling. Spherule growth textures were excentroradial, radial, spherulitic, and parallel grains. Some examples are shown in Figs. 22 and 23. The spherulitic growth resembled the texture of the devitrified spherules. Some of these features, along with

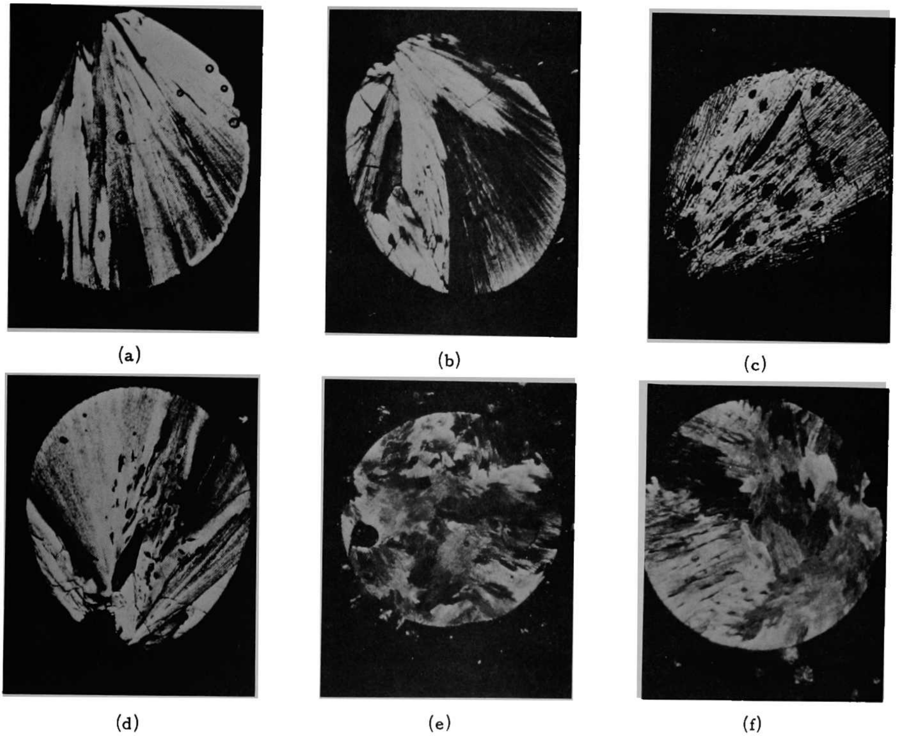

Fig. 22. Photomicrographs of Representative Thin Sections of Spherules Taken with Crossed Nicols Exhibiting Excentroradial and Random-Grain Textures. ANL Neg. No. 308-4101

a. Slice on outer part of spherule EC showing excentroradial texture. The center slice of this spherule exhibited a parallel-grain texture. Furnace temperature 1240°C; estimated nucleation temperature 1285°C.

b. Spherule 24E4 showing excentroradial texture. Furnace temperature 1003°C; estimated nucleation temperature 1070°C.

c. Spherule EG showing excentroradial texture. Furnace temperature 1173°C; estimated nucleation temperature 1180°C.

d. Spherule 24E14 showing excentroradial texture. Furnace temperature 970°C, estimated nucleation temperature 1004°C.

(contd.)

e. Spherule E4 showing random-grain texture and some tendancy for parallel growth. Furnace temperature 1173°C; estimated nucleation temperature 1204°C.

f. Spherule EK showing both random grain and parallel grains. Furnace temperature 1318°C; estimated nucleation temperature 1318°C.

---

other information on furnace temperature, nucleation temperature, the phase diagram of the $MgSiO_4$-SiO_2 system, and the metastable extension of the forsterite liquidus, are displayed in Fig. 24. We conclude from the data in Fig. 24 and our other data that crystal morphologies and sizes, as well as crystal textures, can be correlated with the degree of subcooling.

5. Relation to the Properties of Chondrules

The spherule textures exhibited in Figs. 22 and 23 bear a striking resemblance to those of chondrules. The variety of textures, crystal morphologies and crystal sizes indicate that differences in the degree of supercooling lead to the large variety of textures, crystal morphologies, and crystal sizes observed in chondrules. The measured rates of devitrification of the glasses indicate that chondrules had to have crystallized at temperatures considerably in excess of 600°C and probably in excess of 900°C at some point in their history. Nucleation constraints on the crystallization of a stable phase (*e.g.*, enstatite) led to the formation of a larger amount of forsterite (Mg_2SiO_4) than would be present at equilibrium, and the correct phase diagram is that which includes the metastable extension of the forsterite liquidus shown in Fig. 24 and excludes the enstatite field. The composition of the residual glass never reached the metastable liquidus, presumably because of extremely slow crystallization in these siliceous compositions.

These facts place limitations on current theories of the origin of chondrules. For example, if chondrules were formed by direct condensation to metastable supercooled liquids, they could have formed in a nebula of solar composition at pressures as low as 10^{-3} - 10^{-4} atmospheres. If formed by impact melting during the collision of a "meteorite" (true name on a body with no atmosphere is bolide) with another body, chondrules must have been in a thermal blanket at high temperatures after their formation. Thus, in addition to interest in the phenomenon of supercooling because of the fundamental physical principles involved, the phenomenon appears to have a bearing on the ancient origins of our solar system.

B. Oxygen Isotopes in Refractory Inclusions in Allende
(M. Blander)

Clayton *et al.*[45] have observed anomalous oxygen isotope compositions in the calcium-aluminum-rich inclusions (CAI) in the Allende meteorite. They concluded from their measurements that, contrary to the textural evidence,[46] these inclusions could never have been liquid. This conclusion is contrary to our observations and conclusions from the constrained equilibrium theory.[46] The CAI are refractory and appear to be the most primitive and oldest materials in meteorites. It has been proposed that they are among the earliest condensates

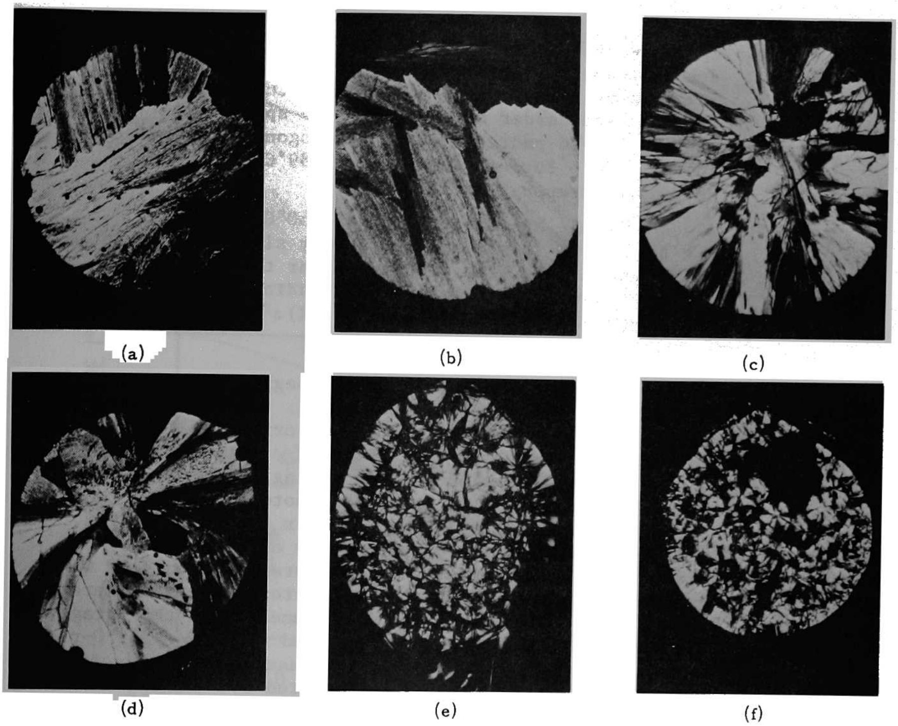

Fig. 23. Photomicrographs of Representative Thin Sections of Spherules Exhibiting Parallel-Grain, Radiating and Spherulitic Textures. ANL Neg. No. 308-4100

a. Spherule 23E9 showing parallel grains. Furnace temperature 1054°C; estimated nucleation temperature 1207°C.

b. Spherule 23E7 showing parallel grains. Furnace temperature 1066°C; estimated nucleation temperature 1172°C.

c. Spherule 24E7 exhibiting radiating texture. The spherule looks strained and is cracked. Furnace temperature 1002°C; approximate nucleation temperature 1062°C.

d. Spherule 23E12 exhibiting radiating texture. Note curved growth of radiating lines which appear to be crystals stacked in a curved succession. Furnace temperature 1042°C, estimated nucleation temperature 1106°C.

(contd.)

e. Spherule 24E9 exhibiting spherulitic texture. There appear to be a large number of nucleation sites leading to many individual spherulites which fill the spherule and border each other. The spherulites exhibit curved radiating lines analogous to those in Fig. 23d. Furnace temperature 989°C; estimated nucleation temperature 1022°C.

f. Glass spherule MB6 devitrified at 950°C for 20 sec. The texture of this spherule is very similar to 24E9 shown in Fig. 23e. There appear to be a number of spherulites with growth radiating from many nucleation sites. (SiO_2 = 58.6%).

---

from a solar nebula and provide direct clues on the beginnings of our solar system. We show that the conclusions of Clayton *et al.* are unwarranted and that their observations are consistent with a liquid origin of the CAI. The observations made by Clayton *et al.* are that plots of δ_{18} *vs.* δ_{17} for separated minerals of a single inclusion fell on a single line of almost a 45° slope. [δ represents the content of an oxygen isotope relative to its content in a standard, *i.e.*, $\left((C_{18}/C_{16})/(C^\circ_{18}/C^\circ_{16})-1\right) \times 1000 = \delta_{18}$.] If, at some stage of nucleosynthesis in the early history of the solar system (or other star system), the helium building process predominated, ^{16}O would predominate. If an early liquid condensate of refractory materials were to later contact ^{17}O- and ^{18}O-containing materials produced in another stage of nucleosynthesis, there would be a diffusion of ^{17}O and ^{18}O into the ^{16}O-rich minerals. Solving the diffusion equations for the case where the isotope effect on diffusion coefficients (D) can be represented by

$$D_{17} = D_{18}(1 + \Delta) \tag{29}$$

where the maximum value of $\Delta = (18/17)^{1/2} - 1 \cong 0.03$, then the isotope effect on δ can be calculated and is given in Table 7 for the case where the minerals are almost equibibrated, where each line in the table represents different

Table 7. Expected Relative Isotope Effects for Δ = 0.03

$-\delta_{18}$	$-\delta_{17}$	$\delta_{18}-\delta_{17}$
40.0	36.86	3.14
30.0	27.41	2.59
20.0	18.05	1.95
10.0	8.85	1.16
1.0	0.83	0.17

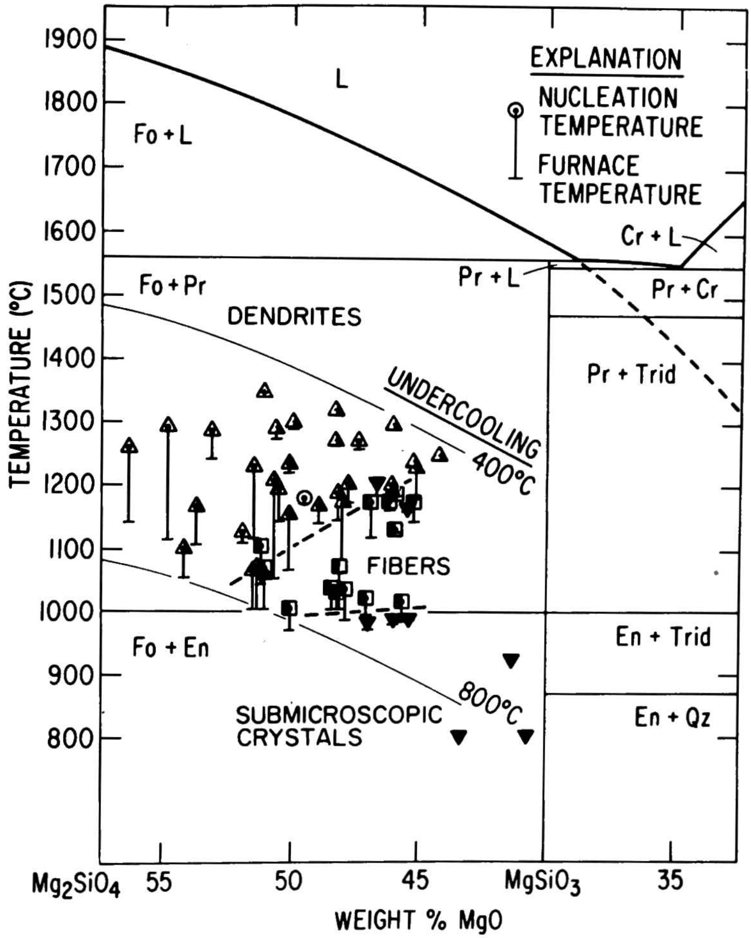

Fig. 24. Crystal Morphologies and Crystal Width Classes that Correspond to the Estimated Nucleation Temperatures of the Magnesium Silicate Spherules. ANL Neg. No. 308-4053

Crystal morphologies: ○, bars; △, dendrites; □, fibers; and ▽, submicroscopic crystals. Crystal width classes: open symbols (*e.g.*, △), fine; right half shaded (*e.g.*, ◮), very fine; left half shaded (*e.g.*, ◭) extremely fine; filled symbols (*e.g.*, ▲), submicroscopic crystals. Short dashed lines separate general temperature-composition fields for morphologies correlated with (Contd.)

nucleation temperature. Equilibrium phase diagram for a portion of the Mg_2SiO_4-SiO_2 system shown for reference. Dotted line illustrates the metastable extension of the forsterite liquidus. Abbreviations: Fo, forsterite; Pr, protoenstatite; En, ortho-enstatite; Cr, cristobalite; Trid, tridymite; Qz, β-quartz; and L, liquid.

---

extents of equilibration. Differences between the degrees of equilibrium of different minerals can arise because of differences in the ratios of (D/a^2) where a is a measure of the average crystal size. Both D and a are known to vary for different minerals in a single CAI and, thus, different minerals would be expected to equilibrate to different extents and have different values of δ. It is remarkable that the measurements of Clayton *et al.*, when normalized relative to a consistent standard, are in accord with the calculated values of Table 7. Their plot of δ_{18} *vs.* δ_{17} deviates from the slope of 45° which their solid mixing model predicts and thus appears to be consistent with our model and inconsistent with theirs.

REFERENCES

1. K. P. Coffin and C. O'Neal, Jr., Experimental Thermal Conductivities of the $N_2O_4 \rightleftarrows 2NO_2$ System, National Advisory Committee for Aeronautics-Technical Note 4209, Washington, D. C., February 1958.

2. J. N. Butler and R. S. Brokaw, J. Chem. Phys. 26, 1636 (1957).

3. J. O. Hirschfelder, C. F. Curtiss and R. B. Bird, Molecular Theory of Gases and Liquids, John Wiley and Sons, Inc., N. Y. (1954), Ch. 8.

4. W. Weltner and K. S. Pitzer, J. Amer. Chem. Soc. 73, 2606 (1951).

5. J. P. Chandler, Physics Dept., Indiana University, Bloomington, Indiana; SIMPLEX is a copyrighted program (Copyright 1965, J. P. Chandler).

6. C. B. Kretschmer and R. Wiebe, J. Amer. Chem. Soc. 76, 2579 (1954).

7. R. Hultgren *et al.*, Selected Values of the Thermodynamic Properties of Binary Alloys, American Society for Metals, Metals Park, Ohio, 44073 (1973).

8. M. S. Foster, S. E. Wood and C. E. Crouthamel, Inorg. Chem. 3, 1428 (1964).

9. JANAF Thermochemical Tables, 2nd Edition, N.B.S. 37, Superintendent of Documents, U.S. Government Printing Office, Washington, D. C. (1971).

10. V. P. Mashovets and L. V. Puchkov, Zh. Prikl. Khim. 38(8), 1875 (1965).

11. H. Reiss, J. Katz and O. J. Kleppa, J. Phys. Chem. 36, 144 (1962).

12. M. Blander and S. J. Yosim, J. Chem. Phys. 39, 2610 (1963).

13. M. L. Saboungi and P. Cerisier, J. Electrochem. Soc. 121, 1258 (1974).

14. S. V. Meschel and O. J. Kleppa, J. Chem. Phys. 48, 5146 (1968).

15. M. Blander, J. Chem. Phys. 34, 432 (1961).

16. M. Blander *et al.*, Physical Inorganic Chemistry Annual Report, July 1973-June 1974, USAEC Report ANL-8123 (1974).

17. M. L. Saboungi and M. Blander, J. Chem. Phys. 63, 212 (1975).

18. M. L. Saboungi, H. Schnyders, M. S. Foster and M. Blander, J. Phys. Chem. 78, No. 11, 1091-1096 (1974).

19. M. Blander *et al.*, Chemical Engineering Division Physical Inorganic Chemistry Semiannual Report, July-December (1972), ANL-7978 (1973).

20. E. W. Dewing, Metallurg. Trans. 1, 2169 (1970).

21. G. N. Papatheodorou, (a) J. Phys. Chem. 77, 472 (1972), (b) Inorg. Chem. 12, 1899 (1973), (c) Z. Anorg. Allg. Chem. 411, 153 (1975).

22. a) T. S. Zvarova, Radiochem. Radioanal. Lett. 11, 113 (1972); b) H. A. Øye and D. M. Gruen, J. Am. Chem. Soc. 91, 2229 (1969).

23. D. M. Gruen and L. R. McBeth, Inorg. Chem. 8, 2625 (1969).

24. P. A. Nelson *et al.*, High Performance Batteries for Off-Peak Energy Storage and Electric-Vehicle Propulsion, Progress Report for the Period July-December 1974, ERDA Report ANL-75-1, Argonne National Laboratory (1975).

25. A. E. Martin, R. K. Steunenberg and Z. Tomczuk, "Changes in the Composition of FeS_2 Electrodes of Li/LiCl-KCl/FeS_2 Cells during Cycling," Extended Abstracts of Electrochemical Society Meeting, New York, October 13-17, 1974, Vol. 74-2, pp 132-133 (1974).

26. R. G. Arnold, Econ. Geol. 57, 72 (1962).

27. G. Urbain, W. Burgman, and M. Frohberg, Acad. Sci. Paris, Ser. C 263, 595 (1966).

28. M. Hansen and K. Anderko, Constitution of Binary Alloys, McGraw-Hill Book Co., New York (1958).

29. P. T. Cunningham, S. A. Johnson, and E. J. Cairns, J. Electrochem. Soc. 119, 1448 (1972).

30. R. G. Arnold, Econ. Geol. 66, 1121 (1971).

31. J. E. Battles and F. C. Mrazek, in Ref. 24.

32. M. I. Homa and B. S. Tani, Argonne National Laboratory, private communication (1974).

33. L. H. Fuchs, Science 153, 166 (1966).

34. D. A. Hansen and J. F. Smith, Acta. Cryst. 24, 913 (1968).

35. K. F. Tebbe *et al.*, Z. Naturforsch. 28b, 600 (1973).

36. F. I. Shamray and P. Ya. Saldau, Izvest. Akad. Nauk S.S.S.R., Otdel. Khim. Nauk 1937, 631.

37. G. Grube, L. Mohr, and L. Breuning, Z. Elektrochem. 41, 880 (1935).

38. K. M. Myles and J. L. Settle, in High Performance Batteries for Off-Peak Energy Storage and Electric-Vehicle Propulsion, Progress Report for the Period January-June 1974, ANL-8109, pp. 64-67 (1975).

39. N. P. Yao, L. A. Heredy, and R. C. Saunders, J. Electrochem. Soc. 118, 1039 (1971).

40. S. P. Yatsenko and E. A. Saltikova, Zh. Fiz. Khim. 48, 2366 (1974).

41. JANAF Thermochemical Tables, Dow Chemical Co., Midland, Michigan (Dec. 31, 1960), and Supplements through Dec. 31, 1974.

42. N. M. Beskorovainyi, V. K. Ivanov, and M. T. Zuev, in High Purity Metals and Alloys, p. 107, V. S. Emel'yanov and A. I. Evstyukhin, Eds., Consultants Bureau, New York (1967).

43. G. Long, in Liquid Alkali Metals, Proc. Int. Conf. on Liquid Alkali Metals, p. 31, British Nuclear Energy Soc., Nottingham (April 1973).

44. M. Blander *et al.*, Chemical Engineering Physical Inorganic Chemistry Semiannual Report, July-December 1972, ANL-7978 (1973).

45. R. N. Clayton, L. Grossman, T. K. Mayeda and N. Onuma, Proceedings of the Soviet American Conference on Cosmochemistry of the Moon and Planets (in press).

46. M. Blander and L. Fuchs, Geochim. Cosmochim. Acta (in press).

X